

## Chapter 2

# Precise Orbit Determination

Adrian Jäggi and Daniel Arnold

**Abstract** Precise Orbit Determination (POD) is an integral part for analyzing measurements from space geodetic techniques such as Satellite Laser Ranging (SLR) and Global Navigation Satellite Systems (GNSS) such as the Global Positioning System (GPS). In the last two decades, POD based on GPS data has furthermore been established as one of the standard techniques to derive trajectories of satellites in the low Earth orbit (LEO) with highest accuracy. Since the launch of dedicated gravity missions, GPS sensors are not only used as a key tracking system for LEO POD, but also for extracting the long wavelength part of the Earth's gravity field (together with SLR to spherical satellites). This chapter introduces SLR and GNSS measurements collected by the terrestrial networks of the International Laser Ranging Service (ILRS) and the International GNSS Service (IGS) as the observational basis for the realization of a terrestrial reference frame from satellite data. On this foundation, the basic equations and mathematical methods of orbit determination are introduced and extensively discussed. Pseudo-stochastic orbit modeling techniques are eventually presented as a general and efficient concept to determine satellite trajectories of highest quality even in presence of deficient force models, covering the full range between dynamic and purely kinematic solutions. Selected results from the application of the discussed orbit determination techniques are highlighted for GPS LEO data. Special emphasis is also put to present orbit determination in the context of more general orbit determination problems, where satellite trajectories are simultaneously determined with other parameters encompassing (at maximum) all pillars of geodesy, i.e., the shape, rotation, and gravity field of the Earth.

---

A. Jäggi (✉) · D. Arnold

Astronomical Institute, University of Bern, Bern, Switzerland  
e-mail: [adrian.jaeggi@aiub.unibe.ch](mailto:adrian.jaeggi@aiub.unibe.ch)

D. Arnold

e-mail: [daniel.arnold@aiub.unibe.ch](mailto:daniel.arnold@aiub.unibe.ch)

© Springer International Publishing AG 2017

M. Naeimi and J. Flury (eds.), *Global Gravity Field Modeling from Satellite-to-Satellite Tracking Data*, Lecture Notes in Earth System Sciences, DOI 10.1007/978-3-319-49941-3\_2

## 2.1 Precise Tracking Data

Precise orbit determination of artificial satellites requires precise measurements which are related to the position or velocity of the satellites. These data are today collected by satellite tracking systems which measure the properties of the propagation of electromagnetic waves between the transmitter and receiver. In this chapter we focus on precise tracking data collected from Global Navigation Satellite Systems (GNSS), Satellite Laser Ranging (SLR), and inter-satellite ranging. For an overview of various (other) tracking systems the reader is referred to, e.g., [104].

### 2.1.1 Global Positioning System

Over the past four decades, the Global Positioning System (GPS) has evolved from a predominantly military navigation system into an indispensable tool not only for society at large, but also for geodetic research and global monitoring of the Earth [106]. Over the past two decades, GPS has also become a unique tool for deriving very precise orbits of satellites in the Low Earth Orbit (LEO). Equipped with onboard GPS receivers, uninterrupted three-dimensional GPS tracking makes it possible to perform LEO orbit determination with unprecedented accuracy by combining the strength of dense GPS measurements with the strength of the dynamic laws, e.g., [64]. Over the past decade, the world of satellite navigation has experienced further dramatic changes: with the Russian GLONASS, a second GNSS has achieved full operational status, GPS is introducing modernized civil navigation signals, and a variety of new navigation constellations are being built up in Asia and Europe [106]. Most of these recent developments are not yet available in current spaceborne receivers, which still rely uniquely on GPS at the time of writing these lecture notes.

The GPS satellites are arranged in six orbital planes which are inclined by about  $55^\circ$  with respect to the Earth's equator and equally separated by  $60^\circ$  on the equator. The satellite orbits are close to circular, with a semi-major axis of about 26 600 km. The orbital revolution period is about 11 h 58 min, which is half a sidereal day. The full constellation of 24 active satellites (currently 32) guarantees that at least four satellites are simultaneously visible at any time and any location on and in the vicinity of the Earth's surface. All GPS satellites are equipped with an ensemble of atomic clocks to generate coherent carriers in the  $L$ -band, e.g., the  $L_1$  and  $L_2$  carriers with wavelengths of  $\lambda_1 \approx 19.0$  cm and  $\lambda_2 \approx 24.4$  cm. Pseudo-random noise codes are generated and modulated on these carriers by the phase modulation technique. For a more detailed description, the reader is referred to, e.g., [60].

### 2.1.1.1 International GNSS Service

By the late 1980s, many organizations had recognized the potential of GPS for geodesy and geodynamics. A test campaign, conducted in summer of 1992, involved the deployment and operation of a global GPS tracking network, the rapid acquisition of observational data and transfer to global data centers (DCs), and the regular data analysis by several analysis centers (ACs). Thanks to the successful operation and to the continuing effort of the large majority of participating organizations, the International GNSS Service (IGS) became an official service of the International Association of Geodesy (IAG) on January 1, 1994 [9]. Since then, more than 200 organizations, agencies, and universities have shared their resources to define international standards and to establish an independent ground segment, which generates high-accuracy products on a best efforts basis with reliability through redundancy. About ten ACs produce precise ephemerides and clocks of all active GPS satellites, Earth rotation parameters (ERP's), coordinates, velocities and clock corrections to GPS time, global ionosphere maps, and station troposphere zenith path delays for the IGS tracking sites. In order to respond to the ongoing modernization of the GPS and to make use of the newly emerging GNSS, the IGS has initiated the Multi-GNSS-EXperiment (MGEX) [106].

### 2.1.1.2 GNSS Observation Equations

GPS receivers collect several types of GPS code observations, e.g., the  $C/A$ -,  $P_1$ -, and  $P_2$ -code observations, and carrier phase observations, denoted as  $L_A$ ,  $L_1$ , and  $L_2$ . The code observation (or pseudo-range) of the satellite  $k$  at time  $T^k$  and registered by the receiver  $i$  at time  $T_i$ , is defined as

$$P_i^k \doteq c (T_i - T^k), \quad (2.1)$$

where  $P_i^k$  is expressed in units of length,  $c$  is the speed of light,  $T_i$  is the arrival (or observation) time of the signal, as measured by the clock of receiver  $i$ , and  $T^k$  is the transmission time of the signal, as measured by the clock of satellite  $k$ .

GPS positioning is thus primarily based on one-way measurements of the signal traveling time. Therefore, a common reference time, the so-called GPS system time [123], has been defined, which is aligned to the international atomic time (TAI) with a constant offset of  $-19$  s. Although the GPS satellites are equipped with atomic clocks, their clocks have a time-varying offset to GPS time. The same holds for GPS receivers, which are usually not equipped with ultra-stable oscillators. Due to the lack of synchronization between transmitter and receiver clocks, one cannot directly derive ranges from the code measurements, which therefore are called pseudo-ranges. Most receivers usually keep their clocks synchronized with respect to GPS time, but there are also receivers with internal clocks, which are not steered to integer seconds of GPS time. As GPS satellite and receiver clocks are usually affected by a drift, both, transmitter and receiver clock offsets, are only valid for a certain epoch.

The pseudo-range  $P_i^k$  may be related to the slant range  $\rho_i^k$ , i.e., to the geometric distance between the receiver  $i$  at signal reception, expressed in GPS time  $t_i$ , and the satellite  $k$  at signal transmission, expressed in GPS time  $t^k$ , as well, and to the delays due to the Earth's atmosphere as

$$P_i^k = \rho_i^k - c \cdot \Delta t^k + c \cdot \Delta t_i + \Delta \rho_{i,trop}^k + \Delta \rho_{i,ion}^k + \varepsilon_{P_i}^k, \quad (2.2)$$

where  $\Delta t^k = T^k - t^k$  is the clock offset of the satellite  $k$  w.r.t. the GPS system time,  $\Delta t_i = T_i - t_i$  is the clock offset of the receiver  $i$  w.r.t. the GPS system time,  $\Delta \rho_{i,trop}^k$  and  $\Delta \rho_{i,ion}^k$  are the signal delays due to the troposphere and ionosphere, expressed in units of length, and  $\varepsilon_{P_i}^k$  is the residual. Further terms such as relativistic corrections have to be included in the term  $\rho_i^k$  to ensure a correct modeling.

The carrier phase observation  $L_A$ ,  $L_1$ , or  $L_2$  corresponding to the code observation is defined as

$$L_i^k \doteq \lambda (\phi_i - \phi^k + N_i^k), \quad (2.3)$$

where  $L_i^k$  is the accumulated carrier phase observation, expressed in units of length,  $\lambda$  is the corresponding wavelength,  $\phi_i$  is the carrier phase of the reference signal generated by the receiver  $i$  at arrival time  $T_i$ ,  $\phi^k$  is the carrier phase of the transmitted signal at transmission time  $T^k$ , and  $N_i^k$  is the initial carrier phase ambiguity, expressed in an integer number of cycles of  $\lambda$ . The carrier phase observation equation may be formulated in analogy to the code observation equation (2.2) as

$$L_i^k = \rho_i^k - c \cdot \Delta t^k + c \cdot \Delta t_i + \Delta \rho_{i,trop}^k - \Delta \rho_{i,ion}^k + \lambda \cdot B_i^k + \varepsilon_{L_i}^k, \quad (2.4)$$

where  $B_i^k$  denotes a constant bias related to the initial carrier phase ambiguity, expressed in cycles. The major difference to the code observation equation (2.2) is the bias term  $B_i^k$ , which consists of the integer-valued initial carrier phase ambiguity  $N_i^k$ , the real-valued non-zero phase difference between  $\phi_i$  and  $\phi^k$  at any common epoch, and the real-valued satellite and receiver specific hardware delays. If the receiver loses lock of the signal, an additional bias term has to be set up due to the discontinuity (cycle slip) in the accumulated carrier phase observations. An additional difference to the code observation equation (2.2) is the opposite sign of the ionospheric refraction term  $\Delta \rho_{i,ion}^k$  due to a phase advance instead of a group delay.

In summary, the observation equations provided by a dual-frequency GPS receiver at a certain observation  $t_i$  may be written as

$$\begin{aligned} P_{i,1}^k &= \tilde{\rho}_i^k + I_i^k + \varepsilon_{P_{1i}}^k \\ P_{i,2}^k &= \tilde{\rho}_i^k + \xi \cdot I_i^k + \varepsilon_{P_{2i}}^k \\ L_{i,1}^k &= \tilde{\rho}_i^k - I_i^k + \lambda_1 \cdot B_{i,1}^k + \varepsilon_{L_{1i}}^k \\ L_{i,2}^k &= \tilde{\rho}_i^k - \xi \cdot I_i^k + \lambda_2 \cdot B_{i,2}^k + \varepsilon_{L_{2i}}^k, \end{aligned} \quad (2.5)$$

where  $P_{i,1}^k, P_{i,2}^k$  are the code observations on both frequencies,  $L_{i,1}^k, L_{i,2}^k$  are the accumulated carrier phase observations on both frequencies, and where  $\tilde{\rho}_i^k$  is the geometric distance between the receiver  $i$  and the satellite  $k$  including the clock off-sets and the tropospheric refraction.  $B_{i,1}^k, B_{i,2}^k$  are the carrier phase bias parameters on both frequencies, and  $\varepsilon_{P_{1i}}^k, \varepsilon_{P_{2i}}^k, \varepsilon_{L_{1i}}^k, \varepsilon_{L_{2i}}^k$  the residuals of all measurements. The ionosphere is a dispersive medium for the  $L$ -band carrier waves broadcasted by the GPS satellites and the ionospheric refraction is thus proportional to  $1/\nu^2$  in first-order approximation of the carrier frequency  $\nu$ . The signal delays  $\Delta\rho_{i,ion}^k$  on both frequencies may therefore be expressed as a function of the  $L_1$ -related ionospheric refraction  $I_i^k$ . The  $L_2$ -related ionospheric refraction then follows by a simple multiplication of  $I_i^k$  by the conversion factor  $\xi = \nu_1^2/\nu_2^2 \approx 1.6469$ .

Because the code observations are two to three orders of magnitude less precise than the carrier phase observations, which exhibit a thermal noise at the level of mm only, the carrier phase observables are primarily used for high-precision geodetic applications. In order to minimize or eliminate specific error sources, such as ionospheric refraction on the right-hand sides of Eq. (2.5), it is common practice to form differences between the original measurements with GPS observations from other receivers (single or double-differences), or to form linear combinations of the original dual-frequency measurements, e.g., the ionosphere-free linear combination, or to combine both techniques. It is, however, also possible to directly process the original (undifferenced) observations from Eq. (2.5) by estimating epoch-wise ionosphere delays, e.g., [163]. For a general discussion and thorough derivation of the GPS observation equations and their linear combinations, e.g., in the context of ambiguity resolution, the reader is referred to [143].

### 2.1.2 Satellite Laser Ranging

The first SLR measurements to a satellite equipped with laser reflectors were collected on 31 October, 1964 at the NASA Goddard Geophysical and Astronomical Observatory, only four years after the first laser was constructed [131]. Since then the SLR technique has evolved to one of the most important space-geodetic techniques for the determination of the terrestrial reference frame, the determination of the Earth's gravity field, and the validation of results from the other space-geodetic techniques such as GNSS and Very Long Baseline Interferometry (VLBI). For a summary of the current achievements of SLR, the reader is referred to, e.g., [137].

SLR measures the round-trip time of flight  $\Delta t_i^k$  of the ultra-short and highly energetic laser pulses transmitted by a ground station  $i$  through a telescope and reflected by special corner cubes onboard of a satellite  $k$  back to the telescope. The two-way time of flight may be transformed into a distance by multiplying the time of flight by the speed of light. Similar to other space-geodetic techniques, a number of corrections need to be made, e.g., due to atmospheric delays, relativistic effects, satellite center-of-mass corrections, laser system offsets, etc. Because the

same electronic time interval counter is used at a ground station to register the emission time of a laser pulse and the reception time of the pulse, the SLR two-way measurements are virtually free of synchronization errors. Focusing on the geometric part and omitting all other terms, the fundamental SLR observation equation reads as

$$\Delta t_i^k = \tau_{i,up}^k + \tau_{i,down}^k = \frac{1}{c} \left( |\mathbf{r}_i(t_{sat} - \tau_{i,up}^k) - \mathbf{r}^k(t_{sat})| + |\mathbf{r}_i(t_{sat} + \tau_{i,down}^k) - \mathbf{r}^k(t_{sat})| \right), \quad (2.6)$$

where  $\Delta t_i^k$  is the sum of the uplink and downlink time of flight of the laser pulse,  $\mathbf{r}_i$  is the inertial position of the laser station  $i$  at emission time  $t_{sat} - \tau_{i,up}^k$  and reception time  $t_{sat} + \tau_{i,down}^k$ , respectively, and  $\mathbf{r}^k$  is the inertial position of the optical phase center at the satellite  $k$  at the reflection time  $t_{sat}$ . Assuming  $\tau_{i,up}^k \approx \tau_{i,down}^k \approx \frac{1}{2} \Delta t_i^k$  the inertial position of the laser station may be approximated as

$$\mathbf{r}_i(t_{sat} \pm \frac{1}{2} \Delta t_i^k) \approx \mathbf{r}_i(t_{sat}) \pm \frac{1}{2} \Delta t_i^k \cdot \dot{\mathbf{r}}_i(t_{sat}). \quad (2.7)$$

Neglecting higher-order terms, the observation equation (2.6) may then be simplified to

$$\Delta t_i^k = \frac{2}{c} |\mathbf{r}_i(t_{sat}) - \mathbf{r}^k(t_{sat})|, \quad (2.8)$$

where the inertial positions  $\mathbf{r}_i$  and  $\mathbf{r}^k$  of the laser station  $i$  and of the satellite  $k$  both refer to the pulse reflection time  $t_{sat}$  at the satellite. The approximation is sufficient for terrestrial laser ranging up to the altitude of GNSS satellites. For time of flight measurements to distant targets, e.g., for Lunar Laser Ranging (LLR), the observation equation (2.6) has to be used.

## 2.2 Orbit Representation

The slant range  $\rho_i^k$  contains the necessary geometric information to perform orbit determination of the satellites tracked by the respective tracking data. When determining a LEO orbit from undifferenced GNSS tracking data, the observation equation (2.5) or their ionosphere-free linear combinations have to be used. The relevant geometric term reads as

$$\rho_{leo}^k = |\mathbf{r}_{leo}(t_{leo}) - \mathbf{r}^k(t_{leo} - \tau_{leo}^k)|, \quad (2.9)$$

where  $\mathbf{r}_{leo}$  is the inertial position of the LEO antenna phase center at GPS time  $t_{leo}$ ,  $\mathbf{r}^k$  is the inertial position of the antenna phase center of GPS satellite  $k$  at GPS time  $t_{leo} - \tau_{leo}^k$ , where  $\tau_{leo}^k$  is the signal traveling time between the two phase centers.

As Earth orbiting satellites are usually extended objects of considerable size, any of its instruments normally is not located at the satellite's center of mass. The motion

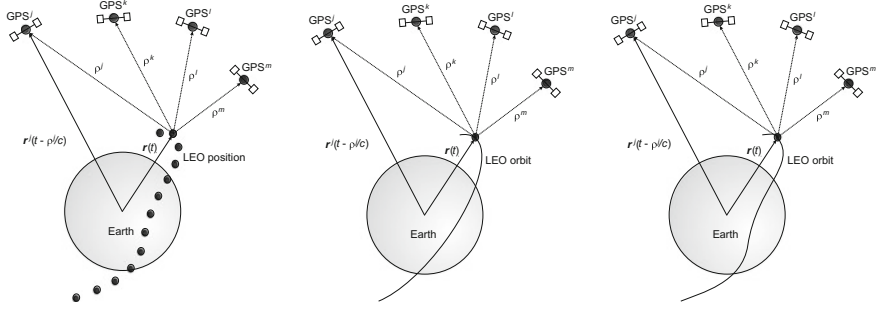


**Fig. 2.1** Kinematic (*left*), dynamic (*middle*), and reduced-dynamic (*right*) orbit representation

of the phase center position of an onboard GNSS antenna or an SLR reflector in inertial space thus comprises the satellite's center of mass motion around the Earth, and the rotation of the satellite body around its center of mass. The orientation of a satellite-fixed coordinate system in inertial space is called the attitude of the satellite. In order to relate the phase center to the center of mass of the LEO spacecraft in inertial space at time  $t_{leo}$ , the location of the antenna phase center position in the satellite-fixed coordinate system and the attitude of the satellite, e.g., as measured by onboard star cameras, have to be known. If both are fulfilled, the LEO center of mass position in Eq. (2.9) may be modeled either by a kinematic, a dynamic, or a reduced-dynamic orbit. The three orbit types are illustrated by Fig. 2.1 for LEO orbit determination from GNSS tracking data and are described in more detail in the following subsections.

### 2.2.1 Kinematic Orbit Representation

Kinematic orbit determination describes the satellite's orbital motion by three Cartesian coordinates, estimated from the tracking data for each measurement epoch. The kinematic representation is not limited to satellite orbits, but can be used for all kinds of moving objects, e.g., cars, ships, aircrafts. The inertial phase center position  $\mathbf{r}_{leo}$  of the onboard antenna is related to the satellite's center of mass by

$$\mathbf{r}_{leo}(t_{leo}) = \mathbf{R}(t_{leo}) \cdot \mathbf{r}_{leo,e,0}(t_{leo}; x_1, y_1, z_1, \dots, x_n, y_n, z_n) + \delta \mathbf{r}_{leo,ant}(t_{leo}), \quad (2.10)$$

where  $\mathbf{R}$  is the transformation matrix from the Earth-fixed to the inertial frame,  $\mathbf{r}_{leo,e,0}$  is the position vector of the LEO center of mass in the Earth-fixed frame,  $x_1, y_1, z_1, \dots, x_n, y_n, z_n$  are the epoch-wise kinematic coordinates, and  $\delta \mathbf{r}_{leo,ant}$  is the antenna phase center offset in the inertial frame.

$\delta \mathbf{r}_{leo,ant}$  is assumed to be known, and is obtained in the inertial frame from given antenna phase center offsets (and variations), and the LEO attitude. The epoch-wise

kinematic coordinates, either of the center of mass or of the phase center of the antenna, are the unknown parameters of the orbit determination and often directly set-up in the Earth-fixed system. Kinematic positions of the antenna phase center may be estimated from the tracking data without the knowledge of the phase center offsets  $\delta \mathbf{r}_{leo,ant}$  and the satellite attitude, which is not possible for the center of mass.

Figure 2.1 (left) shows that a kinematic LEO orbit is a satellite ephemerides provided at the (discrete) measurement epochs of the onboard GNSS receiver. Kinematic positions are derived by geometric means only by a precise point positioning (PPP) approach [167], implying that no position information can be derived for between measurement epochs. No velocity or acceleration information can be directly derived from a kinematic trajectory. This is relevant for gravity field determination from kinematic positions when using the acceleration approach or the energy balance as discussed in Chaps. 4 and 5. Numerical differentiation schemes are inevitable and a proper selection of the associated parameters (filter length, filter degree) is crucial, e.g., [6].

Figure 2.2 shows an extract of a 1-s ephemerides of the GOCE kinematic positions in the SP3 format [122], which provides satellite positions (in km) in the International Terrestrial Reference Frame [1]. Because kinematic positions are always referring to the actual measurement epochs (expressed in Fig. 2.2 in GPS time), they cannot be provided on a completely regular 1 s grid. Also the time tags do not necessarily need to coincide with integer seconds. This is obvious for the GOCE onboard receivers, for which the internal clocks were not steered to integer seconds. If more digits are required for the time tags, clock corrections may be provided in the last column of Fig. 2.2 (expressed in  $\mu\text{s}$ ) to compute the time tags by subtracting the clock corrections from the nominal epochs.

* 2009 11 2 0 0	0.80678020		
PL15 -390.612059	6623.987679	73.104149	193219.797196
* 2009 11 2 0 0	1.80678020		
PL15 -389.240315	6624.166512	65.402457	193219.799413
* 2009 11 2 0 0	2.80678020		
PL15 -387.868014	6624.336133	57.700679	193219.801634
* 2009 11 2 0 0	3.80678020		
PL15 -386.495163	6624.496541	49.998817	193219.803855
* 2009 11 2 0 0	4.80678019		
PL15 -385.121760	6624.647724	42.296889	193219.806059
* 2009 11 2 0 0	5.80678019		
PL15 -383.747819	6624.789703	34.594896	193219.808280
* 2009 11 2 0 0	6.80678019		
PL15 -382.373332	6624.922464	26.892861	193219.810495
* 2009 11 2 0 0	7.80678019		
PL15 -380.998306	6625.046003	19.190792	193219.812692
* 2009 11 2 0 0	8.80678019		
PL15 -379.622745	6625.160329	11.488692	193219.814899
* 2009 11 2 0 0	9.80678018		
PL15 -378.246651	6625.265448	3.786580	193219.817123

**Fig. 2.2** Extract of kinematic GOCE positions at begin of 2 Nov, 2009



Kinematic LEO positions are derived without using any information on the LEO dynamics [151]. Kinematic positions therefore may be used for gravity field determination as pseudo-observations for both alternative (energy balance approach, acceleration approach) and classical gravity field recovery methods (variational equations approach). Reference [46] used for the first time kinematic CHAMP positions and demonstrated that gravity field determination is feasible using the energy balance method [113]. The use of precise kinematic positions stimulated several research groups working on gravity field recovery in the first decade of the 21st century due to the less demanding computational resources than in the case of classical numerical integration techniques, e.g., [149]. For groups using the classical approach, e.g., [11], kinematic positions are attractive, as well, thanks to a much simplified handling of the pseudo-observations compared to the original GNSS tracking data.

Kinematic positions are referred to as pseudo-observations, because they are not original observations but derived from GPS data. Due to the presence of the ambiguity parameters in the GPS carrier phase observation equation (2.4), kinematic positions derived from GPS carrier phase data are furthermore not independent but correlated. Figure 2.3 (left) shows a zoom on 700 epochs of the correlation matrix of the Earth-fixed z-component of GRACE-B kinematic positions. Off-diagonal elements are shown over 200 epochs, which corresponds to slightly more than one revolution period (exactly 100 min due to a 30 s position sampling). As expected, the correlations are decreasing on average for increasing epoch differences. Spots of higher correlations may be recognized, as well, which are related to the satellite crossings of the Earth's equator and are thus occurring twice-per-revolution. The better tracking geometry in these regions ensures a better connection of the GPS carrier phase observations (smaller number of interruptions due to multiple ambiguities) and leads to more correlated kinematic positions. On average the correlations drop on this example day to 51 % after one epoch of 30 s, to 40 % after twenty epochs, to 26 % after forty epochs, and to below 10 % after one hundred epochs. During periods of high correlations, however, values of more than 80 % may still be observed after forty epochs, and even after one hundred epochs correlations may still be as high as 45 %.

Figure 2.3 (right) shows for one example day the residuals for distances between the two GRACE satellites as derived from different GPS-based orbit determinations and biased ranges, which are directly observed by the ultra-precise K-Band ranging system. The best performance (smallest residuals) is obtained for the solution 'PHASE', where the original GPS carrier phase data are directly used as observations for a reduced-dynamic orbit determination (see Sect. 2.2.3 for more details on reduced-dynamic orbit determination). For solution 'KIN-EPO', where the same reduced-dynamic orbit parameters are solved from kinematic positions used as pseudo-observations with only epoch-wise covariance information taken into account for the observation weighting in the least-squares adjustment, a significant degradation is obtained. It is obviously not sufficient to only take into account an epoch-wise weighting in the least-squares adjustment, because long-period variations of the kinematic positions are then erroneously fitted by the parameters of the reduced-dynamic orbit model instead of being interpreted as a pure consequence of

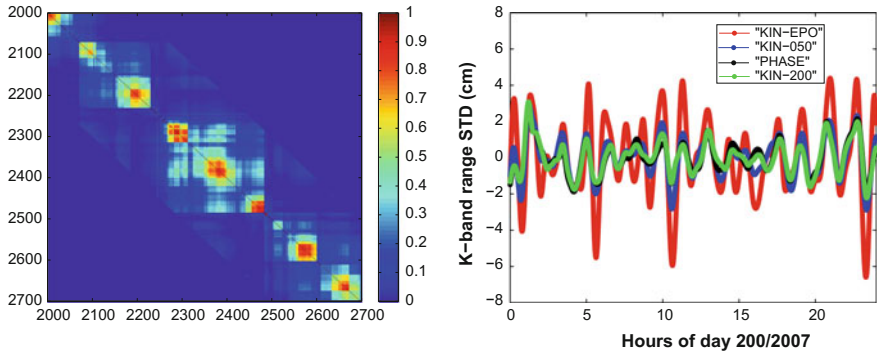


**Fig. 2.3** Extract of correlation matrices of the Earth-fixed z-component of GRACE-B kinematic positions for one example day (*left*) and K-band range residuals for distances between reduced-dynamic GRACE-A and -B orbits stemming from different observation handling (*right*). Figures from [70]

the ambiguity-induced correlations in time. For solutions ‘KIN-50’ and ‘KIN-200’, where covariances over 50 and 200 epochs are taken into account for the observation weighting, respectively, a considerable improvement of the orbit quality is achieved. Solution ‘KIN-200’ shows in essence the same quality as the ‘PHASE’ solution. It has to be emphasized that it is necessary to take into account the rather large number of 200 off-diagonal blocks to achieve a close equivalence to the ‘PHASE’ solution.

Similar to orbit determination, covariance information from the kinematic positioning has also to be taken into account to obtain equivalent results for gravity field recovery as from original GPS carrier phase data [70]. To further exploit kinematic positions for gravity field recovery, empirically derived covariance information is sometimes taken into account in addition [163].

## 2.2.2 Dynamic Orbit Representation

Dynamic orbit determination describes the motion of the satellite’s center of mass as a particular solution of an equation of motion. As real satellite trajectories are always particular solutions of an equation of motion, a dynamic orbit representation is certainly the most natural choice for modeling orbital motion. In dynamic orbit determination, the phase center of the onboard antenna is related to the satellite’s center of mass as

$$\mathbf{r}_{leo}(t_{leo}) = \mathbf{r}_{leo,0}(t_{leo}; a, e, i, \Omega, \omega, u_0; Q_1, \dots, Q_d) + \delta \mathbf{r}_{leo,ant}(t_{leo}), \quad (2.11)$$

where  $\mathbf{r}_{leo,0}$  is the LEO center of mass position in the inertial frame,  $a, e, i, \Omega, \omega, u_0$  are six LEO orbital elements,  $Q_1, \dots, Q_d$  are additional LEO dynamical orbit para-

meters, and  $\delta \mathbf{r}_{leo,ant}$  is the antenna phase center offset with respect to the center of mass in the inertial frame.

In analogy to Eq. (2.10),  $\delta \mathbf{r}_{leo,ant}$  is considered as known. The unknown parameters are the LEO initial osculating orbital elements  $O_j$ ,  $j = 1, \dots, 6$ , and additional dynamical orbit parameters  $Q_1, \dots, Q_d$ . The latter may be scaling factors of analytically or numerically known accelerations, e.g., derived from a model of the Earth's gravity field, or non-gravitational accelerations as measured by an on-board accelerometer.

In a dynamic orbit representation the LEO center of mass position  $\mathbf{r}_{leo,0}$  is modeled as a particular solution of an equation of motion. Dynamic force models are used to describe the equation of motion and to propagate the satellite's center of mass position and velocity over time by numerical integration techniques. Figure 2.1 (middle) shows that a dynamic LEO orbit derived from GNSS tracking data therefore provides a satellite ephemerides, which may be evaluated at any epoch within the orbital arc. By construction, the orbital trajectory is fully dependent on the underlying force models. The equation of motion of an Earth-orbiting satellite including all perturbations reads

$$\ddot{\mathbf{r}} = -GM \frac{\mathbf{r}}{r^3} + \mathbf{f}_p(t, \mathbf{r}, \dot{\mathbf{r}}, Q_1, \dots, Q_d) \doteq \mathbf{f} \quad (2.12)$$

with the initial conditions

$$\mathbf{r}(t_0) = \mathbf{r}(a, e, i, \Omega, \omega, u_0; t_0) \quad \text{and} \quad \dot{\mathbf{r}}(t_0) = \dot{\mathbf{r}}(a, e, i, \Omega, \omega, u_0; t_0), \quad (2.13)$$

where  $GM$  is the gravity constant times the mass of the Earth,  $\mathbf{r}$  the geocentric position of the satellite in the inertial frame,  $\mathbf{f}_p$  the perturbing acceleration acting on the satellite in the inertial frame, and  $\mathbf{f}$  the total acceleration. The acceleration  $\mathbf{f}_p$  comprises all modeled gravitational and non-gravitational perturbations. The force models used may explicitly depend on the time  $t$ , or implicitly through the position vector  $\mathbf{r}$  and the velocity vector  $\dot{\mathbf{r}}$  of the satellite, as well as on additional force model parameters  $Q_1, \dots, Q_d$  that need to be adjusted.

At least one set of initial conditions (initial osculating elements) is estimated from the tracking data in a dynamic orbit determination procedure. Figure 2.4 illustrates the orbit represented by the six initial osculating elements (Keplerian elements)  $a$ ,  $e$ ,  $i$ ,  $\Omega$ ,  $\omega$ , and  $u_0$  at time  $t_0$ . The semi-major axis  $a$  and the numerical eccentricity  $e$  describe the orbit's size and shape, the inclination  $i$  and the right ascension  $\Omega$  of the ascending node describe the orbital plane with respect to the Earth's equator, the argument  $\omega$  of the perigee  $\varPi$  describes the orbit's orientation, and the argument of latitude  $u_0$  describes the satellite's position at time  $t_0$ . These six initial osculating elements are equivalent to the coordinates of the initial position and velocity vectors (state vector) at time  $t_0$  as indicated by Eq. (2.13). The formulas of the two-body problem are conventionally used to relate one set of osculating orbital elements to the state vector and vice versa [7].

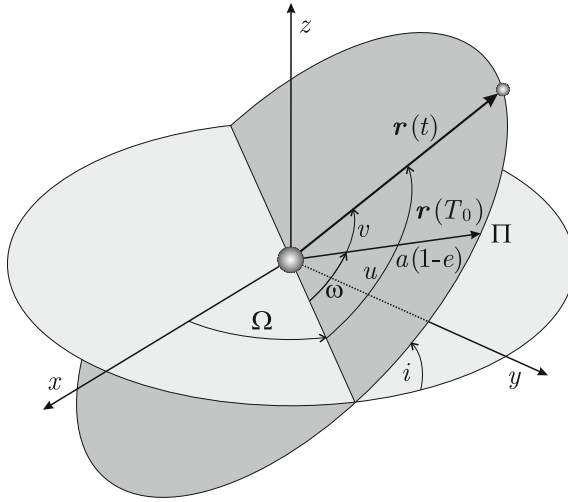


**Fig. 2.4** Initial osculating elements  $a$ ,  $e$ ,  $i$ ,  $\Omega$ ,  $\omega$ , and the argument of latitude  $u$ . Figure from [7]

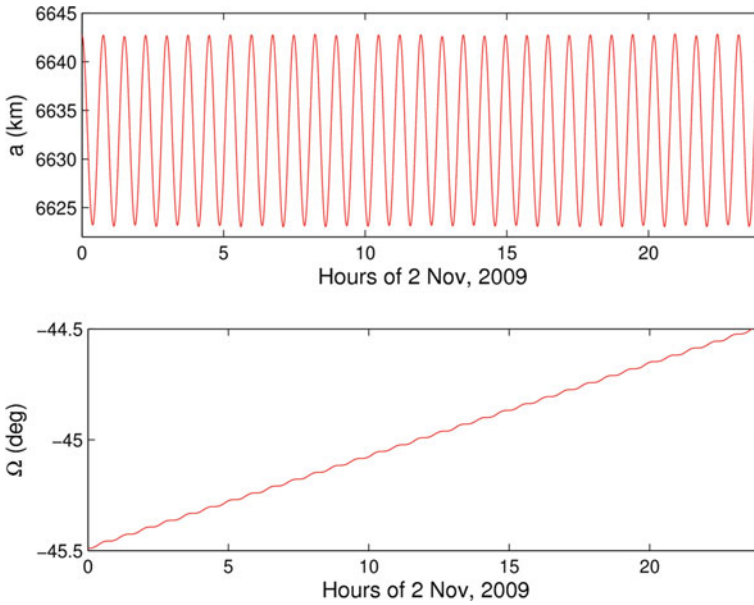


**Fig. 2.5** Osculating semi-major axis (*top*) and right ascension of ascending node of the GOCE orbit on 2 Nov, 2009

Figure 2.5 illustrates the time evolution of the osculating semi-major axis  $a$  (top) and the right ascension  $\Omega$  (bottom) of the ascending node of the GOCE orbit. The full force field was used to propagate the GOCE orbit by numerical integration over

one day and to compute osculating elements from the obtained position and velocity vectors. The observed variations are mainly due to the oblateness of the Earth [8]. Figure 2.5 (top) shows twice-per-revolution periodic variations with an amplitude of about 10km around a mean semi-major axis of 6632.9km, which corresponds to a mean GOCE orbital altitude of 254.9km. Apart from small twice-per-revolution periodic variations, Fig. 2.5 (bottom) shows a pronounced linear drift of  $\approx 1^\circ/\text{day}$  ( $360^\circ/365$  days). The node advances, because the inclination of the GOCE orbit is about  $96^\circ > 90^\circ$ , which in turn is required to maintain the sun-synchronous GOCE orbit. Both effects shown in Fig. 2.5 are mainly due to the oblateness of the Earth and can be explained by solving the Gaussian perturbation equations by first order perturbation theory, see e.g., [7].

### 2.2.3 Reduced-Dynamic Orbit Representation

The real-world dynamics of LEO satellites is not known to the precision required by highly precise tracking data such as GPS or K-band observations. Therefore, the concept of reduced-dynamic orbit determination has already been introduced several decades ago to better exploit precise tracking data such as GPS carrier phase measurements, [161, 162]. Reduced-dynamic orbits are accomplished by complementing the deterministic orbit model by additional stochastic parameters, which are adjusted together with the deterministic orbit parameters.

Pseudo-stochastic orbit modeling as presented in this chapter may be considered as a particular realization of the reduced-dynamic orbit determination technique and is discussed according to [64]. It makes use of both the geometric strength of GNSS observations and that satellite trajectories are particular solutions of a deterministic equation of motion. The attribute ‘pseudo’ distinguishes this method from stochastic orbit modeling where a satellite trajectory is modeled as a solution of a stochastic differential equation [73]. Pseudo-stochastic orbit modeling, in contrast, introduces additional empirical parameters  $P_1, \dots, P_s$ , subsequently referred to as pseudo-stochastic orbit parameters, to the deterministic equation of motion (2.12), which then reads as

$$\ddot{\mathbf{r}} = -GM \frac{\mathbf{r}}{r^3} + \mathbf{f}_p(t, \mathbf{r}, \dot{\mathbf{r}}, Q_1, \dots, Q_d, P_1, \dots, P_s) \doteq \mathbf{f}. \quad (2.14)$$

The attribute ‘stochastic’ arises from the practice to optionally characterize these additional parameters by a priori known statistical properties like, e.g., expectation values and a priori weights, which constrain the estimated parameters to user-specified expectation values.

Figure 2.1 (middle, right) shows that a (reduced-) dynamic LEO orbit is a satellite ephemerides, which may be evaluated at any epoch within the orbital arc. Consequently reduced-dynamic positions can be provided on a regular grid as requested by the SP3 format and illustrated in Fig. 2.6, which shows an extract of a 10s

* 2009 11 2 0 0	0.00000000			
PL15 -391.718353	6623.836682	79.317661	999999.999999	
VL15 13710.157683	1908.731015	-77015.601314	999999.999999	
* 2009 11 2 0 0	10.00000000			
PL15 -377.980705	6625.284690	2.298385	999999.999999	
VL15 13764.602016	987.250587	-77021.193676	999999.999999	
* 2009 11 2 0 0	20.00000000			
PL15 -364.190222	6625.811136	-74.721213	999999.999999	
VL15 13815.825127	65.631014	-77016.232293	999999.999999	
* 2009 11 2 0 0	30.00000000			
PL15 -350.350131	6625.415949	-151.730567	999999.999999	
VL15 13863.820409	-855.995477	-77000.719734	999999.999999	
* 2009 11 2 0 0	40.00000000			
PL15 -336.463660	6624.099187	-228.719134	999999.999999	
VL15 13908.581905	-1777.497047	-76974.660058	999999.999999	
* 2009 11 2 0 0	50.00000000			
PL15 -322.534047	6621.861041	-305.676371	999999.999999	
VL15 13950.104280	-2698.741871	-76938.058807	999999.999999	
* 2009 11 2 0 1	0.00000000			
PL15 -308.564533	6618.701833	-382.591743	999999.999999	
VL15 13988.382807	-3619.598277	-76890.923043	999999.999999	

**Fig. 2.6** Extract of reduced-dynamic GOCE positions at begin of 2 Nov, 2009

ephemerides of GOCE reduced-dynamic positions and velocities (expressed in dm/s). Opposed to a purely dynamic orbit, the reduced-dynamic solution is more data-driven due to the empirical parameters and to a certain extent allowed to follow ‘excursions’ which otherwise are not described by the force models. Consequently, the highly accurate tracking data may be better fitted and reduced-dynamic approaches are therefore potentially well suited to compute LEO orbits of highest quality also in the presence of deficient force models. The empirical parameters may compensate unmodeled non-gravitational forces and even cope with rapidly changing accelerations as subsequently illustrated. Depending on the actual parametrization, the orbital trajectories nevertheless still heavily depend of the underlying force models. Reduced-dynamic positions are therefore not recommended to, e.g., serve as pseudo-observations for a subsequent and independent recovery of the Earth’s gravity field [65].

Figure 2.7 shows the estimated empirical parameters of a reduced-dynamic orbit determination of the GOCE satellite in the commissioning phase on 7 May, 2009. The empirical parameters are set up as piecewise constant accelerations over 6 min (see Sect. 2.3.2.2) and mainly compensate the not explicitly modeled atmospheric drag experienced by the satellite. The changes in the signature of the estimated along-track accelerations in the middle of the day are related to the commissioning of the ion propulsion assembly of the GOCE satellite. Due to the unexpectedly low drag during the commissioning phase in spring 2009, GOCE was switched into the science mode on this day. Two thrust biases of 4 mN at maximum and follow-up biases of about 2–2.5 mN brought the satellite into the first drag-free flight ever. Figure 2.7 (middle) illustrates that the along-track drag is compensated to a large extent during this first

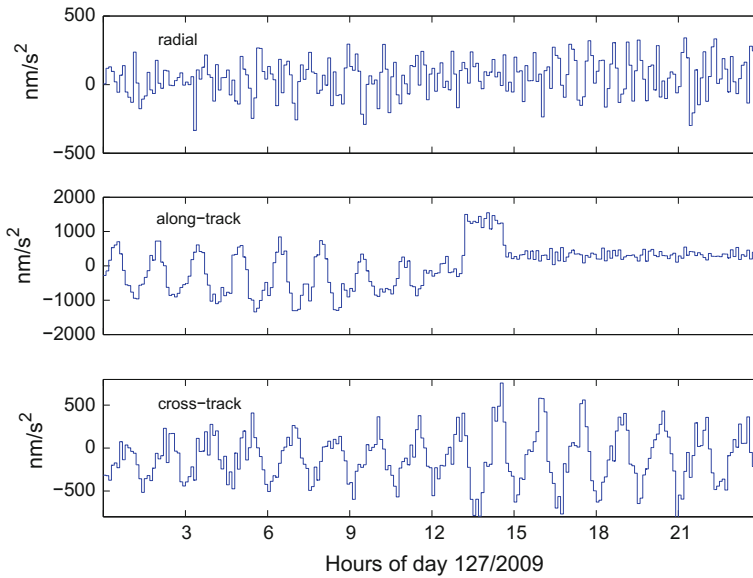


**Fig. 2.7** Piecewise constant accelerations of a reduced-dynamic GOCE trajectory during the commissioning phase. Figure from [68]

drag-free flight. Remaining variations were reduced to a magnitude similar to the accelerations experienced in the radial direction. However, due to the extremely low atmospheric density at that time and altitude, a closed-loop drag-free flight was not yet feasible for a longer period than a couple of days. A next, slightly longer test was again started 26 May, 2009, at an altitude of about 272.5 km, but only after having reached the final orbital altitude of 259.56 km (mean spherical altitude, 254.9 km when referring to the mean semi-major axis), the GOCE satellite was eventually brought in the closed-loop drag-free flight on 14 September, 2009, e.g., [68].

### 2.2.4 Orbit Comparison

The characteristics of kinematic and reduced-dynamic orbits may be further illustrated by forming differences between them. This is a widely used technique to internally assess the consistency between the two types of orbits, e.g., [18, 145]. Although the differences do not give direct information about the orbit accuracy, they are a good indicator for the GPS data quality, e.g., in terms of noise and data outages, because kinematic positions are particularly sensitive to these issues.

Figure 2.8 shows the differences between GOCE kinematic positions and a reduced-dynamic GOCE ephemerides for a 30 h arc in the early phase of the mission as an example. The differences can only be computed at the discrete epochs of the



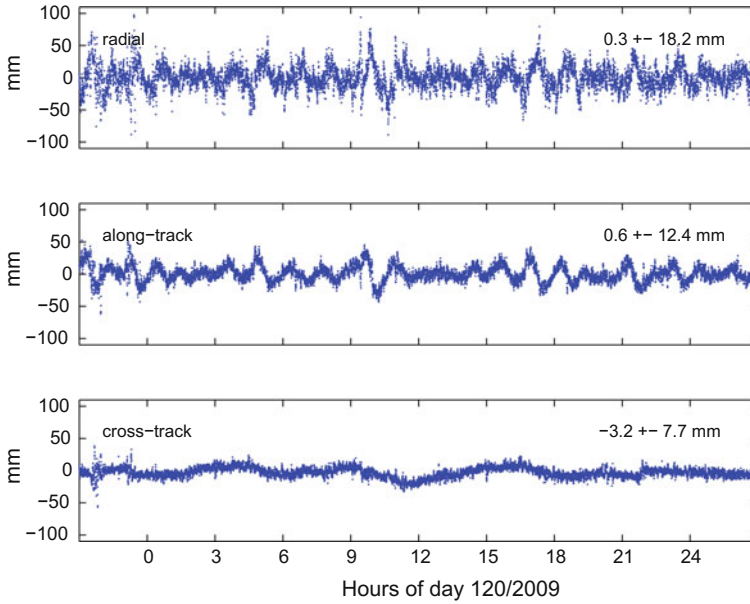


**Fig. 2.8** Differences of GOCE kinematic positions with respect to a reduced-dynamic trajectory

kinematic positions, and are then transformed into the radial, along-track and cross-track directions as derived from the reduced-dynamic trajectory. Figure 2.8 shows that the two GOCE orbits agree on a level of a few centimeters. The scatter in the differences is due to the kinematic positions, which are derived without any smoothing or constraints between subsequent epochs. The high-frequency position noise is thus mainly given by the GPS carrier phase noise. It is largest in the radial (‘height’) direction due to the simultaneous estimation of kinematic positions and receiver clock corrections at every measurement epoch. The low-frequency variations seen in Fig. 2.8 may be caused by both types of orbits. Possible reasons are systematic carrier phase errors, e.g., receiver antenna phase center variations (PCVs), which are affecting kinematic and reduced-dynamic orbits differently [66], dynamic model errors which may not be fully compensated by the adopted empirical parametrization of the reduced-dynamic orbit [48], or colored noise of the kinematic positions [70]. The mean offsets between the kinematic and reduced-dynamic orbits are very small, which is due to the particular parametrization adopted to the reduced-dynamic orbit, where constant empirical accelerations acting over the entire orbital arc are estimated [66].

It should be emphasized that each additional (empirical) parameter introduced into the reduced-dynamic orbit determination weakens the solution for the other (non-empirical) parameters. Thanks to continuously improving models describing the gravitational, but in particular also the non-gravitational forces acting on LEO satellites, e.g., due to better descriptions via macro-models or direct measurements



of the surface forces by onboard accelerometers, purely empirical parameters can be estimated with tighter constraints (see Sect. 2.3.3) to yield a better dynamic stiffness of the reduced-dynamic trajectories while still providing high quality orbits [41, 49, 146]. In the case of the GOCE mission, the excellent quality of the onboard accelerometers even allowed to completely avoid any empirical parameters and to perform purely dynamic orbit determination on a very good quality level [148].

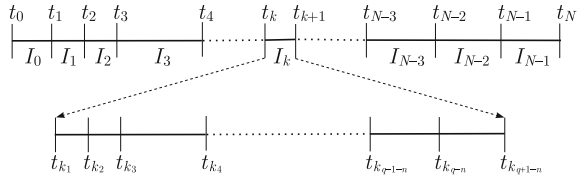
## 2.3 Orbit Determination

Kinematic positioning can be used for a wide range of applications because no conditions are imposed on the receiver motion. Kinematic positions are, however, very sensitive to bad measurements, unfavorable viewing geometry, and data outages. Kinematic positioning is therefore essentially restricted to LEO orbit determination based on spaceborne GNSS tracking data, or to GNSS orbit determination using tracking data of the terrestrial IGS ground network [151]. Dynamic and reduced-dynamic orbit determination, in contrast, make use of physical models of the satellite motion. The underlying orbit determination techniques are therefore also applicable to tracking systems which only sparsely cover an orbital arc with measurements, e.g., as in case of SLR [138]. In the case of GNSS-based LEO orbit determination the dynamic and reduced-dynamic approaches allow for some kind of ‘averaging’ the large number of measurements from different epochs, which makes the resulting position estimates much less prone to bad measurements and data outages. Satellite trajectories can therefore be reasonably well propagated across data gaps, especially if good dynamic models are available. This section has the focus on technical aspects of dynamic and reduced-dynamic orbit determination, introduces the primary equations, the variational equations, and the parameter estimation methods needed for the mathematical description of dynamic and reduced-dynamic orbit determination.

### 2.3.1 Primary Equations

According to Sects. 2.2.2 and 2.2.3 satellite motion is described as a particular solution of an equation of motion when using a dynamic or reduced-dynamic orbit representation. Equations (2.12) and (2.14) are often referred to as the primary equations of the underlying orbit determination problem. The acceleration  $\mathbf{f}_p$  encompasses all gravitational and non-gravitational perturbations. Often, the perturbation model consists of a known part with accelerations given by analytical models, and of a part which includes force model parameters to be adjusted in the course of orbit determination. An overview of models typically taken into account for high-precision dynamic orbit determination is given in [8].

**Fig. 2.9** Subdivision of the integration interval  $I_k$  for collocation algorithm. Figure from [7]



### 2.3.1.1 Numerical Integration

The high accuracy required for precise orbit determination may only be achieved by using numerical integration methods for the solutions of the primary (and the variational) equations. A variety of methods exists, among them well known methods such as Runge-Kutta, multi-step, and extrapolation methods, which have been successfully applied to orbit determination problems. For a detailed overview, we refer to original textbooks and articles published on the subject, e.g., [24, 132], or on textbooks providing overviews and detailed comparisons of methods, e.g., [7, 104].

In this section we give a short overview of the collocation methods as they are used in the Bernese GNSS Software [29] for the numerical integration of satellite orbits [7]. They approximate the initial value problems (2.12) and (2.14) by a polynomial of degree  $q$ , which is substantially higher than the order  $n = 2$  of the underlying differential equation systems (for  $q = n$  the method reduces to the algorithm already developed by Leonhard Euler in 1768, often referred to as the Euler method). The polynomial degree  $q$  is called the order of the method. Orders up to about 10 to 14 typically make sense in a double precision floating point environment. The interval subdivision (see Fig. 2.9) and the definition of the initial value problems at the left interval boundaries are the same as in the Euler method, except that the collocation method of order  $q$  of the previous interval is used to define the new initial values.

The initial value problem referring to the interval  $I_k$ ,  $k = 0, \dots, N - 1$  may be written as

$$\ddot{\mathbf{r}}_k = \mathbf{f}(t, \mathbf{r}_k, \dot{\mathbf{r}}_k) \quad (2.15)$$

with the initial conditions

$$\mathbf{r}_k(t_k) \doteq \mathbf{r}_{k0} \quad \text{and} \quad \dot{\mathbf{r}}_k(t_k) \doteq \dot{\mathbf{r}}_{k0} , \quad (2.16)$$

where the initial values are defined for  $i = 0, 1$  as

$$\mathbf{r}_{k0}^{(i)} = \begin{cases} \mathbf{r}_0^{(i)} & ; k = 0 \\ \mathbf{r}_{k-1}^{(i)}(t_k) & ; k > 0 \end{cases} . \quad (2.17)$$

The collocation algorithm of order  $q$  approximates the initial value problem (2.15) in the interval  $I_k = [t_k, t_{k+1}]$  by a polynomial of degree  $q$  as

$$\mathbf{r}_k(t) \doteq \sum_{l=0}^q \frac{1}{l!} (t - t_k)^l \mathbf{r}_{k0}^{(l)}, \quad (2.18)$$

where the coefficients  $\mathbf{r}_{k0}^{(l)}$ ,  $l = 0, \dots, q$  are obtained by requesting that the numerical solution assumes the initial values (2.17) and that the numerical solution solves the differential equation system at exactly  $q - 1$  different epochs  $t_{k_j}$ ,  $j = 1, \dots, q - 1$ , within the interval  $I_k$  (see Fig. 2.9 for  $n = 2$ ).

Whereas the first conditions are automatically met by the definition of Eq. (2.18), the second conditions are obtained by replacing  $\mathbf{r}_k(t)$  (and its time derivatives) in the differential equation system (2.15) by Eq. (2.18) for the epochs  $t_{k_j}$ , which yields

$$\sum_{l=2}^q \frac{(t_{k_j} - t_k)^{l-2}}{(l-2)!} \mathbf{r}_{k0}^{(l)} = \mathbf{f}(t_{k_j}, \mathbf{r}_k(t_{k_j}), \dot{\mathbf{r}}_k(t_{k_j})) \quad , \quad j = 1, \dots, q - 1. \quad (2.19)$$

The above mentioned condition equations are algebraic and in general non-linear in the unknowns  $\mathbf{r}_{k0}^{(l)}$ ,  $l = 2, \dots, q$ , because they also implicitly show-up on the right-hand sides of Eq. (2.19), where the terms  $\mathbf{r}_k^{(i)}(t_{k_j})$  must be replaced by the right-hand sides of Eq. (2.18). The number of unknowns is equal to the number of condition equations. An efficient solution strategy based on an iterative approach may be found in [7].

Whereas the above mentioned integration technique may be used without any difficulty to represent orbital arcs with much better precision than required by ‘classical’ tracking data such as GPS carrier phase measurements or SLR data, it is not trivial to generate solutions of the initial value problem (2.15) from which inter-satellite distances may be derived with an accuracy of about  $1 \mu\text{m}$  for arcs as long as one day. In order to guarantee accuracies of better than  $1 \mu\text{m}$  for inter-satellite distances as requested for K-band inter-satellite ranging, the collocation procedures need to be modified to represent the initial state vectors associated with the subintervals with better than double precision when keeping the arclength of one day. For details the reader is referred to [11].

In view of the prospect that the micrometer-precise K-band ranging instrument onboard the future GRACE Follow-On mission will be supplemented by a 50–100 nm precise precise laser interferometer [133], it is clear that future gravity missions relying on ultra-precise inter-satellite ranging observables will pose even higher demands on the numerical integration techniques used to represent the satellite trajectories. A recent study based on a full-scale closed-loop simulation for a GRACE Follow-On type pair of satellites using inter-satellite laser ranging underlined that a standard processing with double precision may indeed be a limiting factor for exploiting the nm precision of a laser interferometer to its full extent and proposed a scheme with enhanced precision that uses both double and quadruple precision in different parts of the processing chain [31].

### 2.3.1.2 Orbit Improvement

Let us assume that an a priori orbit  $\mathbf{r}_0(t)$  is available, which is represented by the (a priori) parameter values  $P_{0,i}$ . Such an orbit may be realized, e.g., by a dynamical fit of LEO positions obtained from a kinematic solution using GPS code measurements, or from an extrapolation of an orbit trajectory covering the previous day. Orbit determination discussed in this chapter is therefore understood as an orbit improvement process, where the actual orbit  $\mathbf{r}(t)$  is expressed as a truncated Taylor series with respect to the unknown orbit parameters  $P_i$  about the a priori orbit as

$$\mathbf{r}(t) = \mathbf{r}_0(t) + \sum_{i=1}^n \frac{\partial \mathbf{r}_0}{\partial P_i}(t) \cdot (P_i - P_{0,i}) , \quad (2.20)$$

where  $n = 6 + d$  denotes the total number of orbit parameters and  $\frac{\partial \mathbf{r}_0}{\partial P_i}(t)$  describes the orbital change due to a change in the parameter  $P_i$ . Provided that the orbit parameter corrections  $p_i = P_i - P_{0,i}$ , e.g., derived from a least-squares adjustment of spacecraft tracking data as discussed in Sect. 2.3.3, and the partial derivatives of the a priori orbit with respect to the orbit parameters are known, Eq. (2.20) allows it to improve the a priori orbit. The trajectory (2.20) should be called the ‘linearized’ solution of the original (non-linear) orbit determination problem. Alternatively, it is possible to use the dynamic models together with the improved dynamical parameters to propagate the improved initial state vector by numerical integration. Strictly speaking, however, the latter approach is not fully consistent to the improved orbit parameters.

### 2.3.2 Variational Equations

Knowledge of the partial derivatives of the a priori orbit with respect to the estimated parameters as a function of time is required for orbit improvement. Let us assume that  $P_i$  is one of the parameters defining the initial conditions or the dynamics in the equation of motion (2.12), and that the partial derivative of the a priori orbit  $\mathbf{r}_0(t)$  with respect to this parameter is designated by the function

$$\mathbf{z}_{P_i}(t) \doteq \frac{\partial \mathbf{r}_0}{\partial P_i}(t) . \quad (2.21)$$

The initial value problem associated with the partial derivatives (2.21) is obtained by taking the partial derivative of the equation of motion (2.12). The result is subsequently referred to as the variational equation of parameter  $P_i$ , which is obtained by adopting the ‘chain rule’ and reads as

$$\ddot{\mathbf{z}}_{P_i} = \mathbf{A}_0 \cdot \mathbf{z}_{P_i} + \mathbf{A}_1 \cdot \dot{\mathbf{z}}_{P_i} + \frac{\partial \mathbf{f}_p}{\partial P_i}, \quad (2.22)$$

with the  $3 \times 3$  (Jacobian) matrices defined by

$$A_{0[i;k]} \doteq \frac{\partial f_i}{\partial r_{0,k}} \quad \text{and} \quad A_{1[i;k]} \doteq \frac{\partial f_i}{\partial \dot{r}_{0,k}}, \quad (2.23)$$

where  $f_i$  denotes the component  $i$  of the total acceleration  $\mathbf{f}$  from (2.12) and  $r_{0,k}$  denotes the component  $k$  of the geocentric position from (2.12).

For  $P_i \in \{a, e, i, \Omega, \omega, u_0\}$  the variational equations (2.22) are a linear, homogeneous differential equation system of second order in time with initial values  $\mathbf{z}_{P_i}(t_0) \neq \mathbf{0}$  and  $\dot{\mathbf{z}}_{P_i}(t_0) \neq \mathbf{0}$ . For  $P_i \in \{Q_1, \dots, Q_d\}$  (2.22) are inhomogeneous, but have zero initial values because the initial satellite state does not depend on the force model parameters. It is important that the homogeneous part of (2.22) is the same for dynamical parameters and for parameters defining the initial conditions, which allows for an efficient solution process.

### 2.3.2.1 General Solution

Let us assume that the functions  $\mathbf{z}_{O_j}(t)$ ,  $j = 1, \dots, 6$  are the partial derivatives of the a priori orbit  $\mathbf{r}_0(t)$  with respect to the six parameters  $O_j$ ,  $j = 1, \dots, 6$  defining the initial conditions at time  $t_0$ . The ensemble of these six functions forms one complete system of solutions of the homogeneous part of the variational equation (2.22), which allows us to obtain the solution of the inhomogeneous system by the method of ‘variation of constants’. The solution and its first time derivative may thus be written as a function of the homogeneous solutions  $\mathbf{z}_{O_j}(t)$  as

$$\mathbf{z}_{P_i}^{(k)}(t) = \sum_{j=1}^6 \alpha_{O_j P_i}(t) \cdot \mathbf{z}_{O_j}^{(k)}(t); \quad k = 0, 1, \quad (2.24)$$

with the coefficient functions defined by

$$\alpha_{P_i}(t) \doteq \int_{t_0}^t \mathbf{Z}^{-1}(t') \cdot \mathbf{h}_{P_i}(t') \cdot dt', \quad (2.25)$$

where  $\alpha_{P_i}$  denotes the column array  $(\alpha_{O_1 P_i}, \dots, \alpha_{O_6 P_i})^T$ ,  $\mathbf{Z}$  denotes the  $6 \times 6$  matrix defined by  $\mathbf{Z}_{[1, \dots, 3; j]} \doteq \mathbf{z}_{O_j}$ ,  $\mathbf{Z}_{[4, \dots, 6; j]} \doteq \dot{\mathbf{z}}_{O_j}$ , and  $\mathbf{h}_{P_i}$  denotes the column array  $(\mathbf{0}^T, \partial \mathbf{f}_p / \partial P_i)^T$ .

The solution  $\mathbf{z}_{P_i}(t)$  of the variational equation (2.22) and its first time derivative may be expressed with the same functions  $\alpha_{O_j P_i}(t)$  as a linear combination with the homogeneous solutions  $\mathbf{z}_{O_j}(t)$  and  $\dot{\mathbf{z}}_{O_j}(t)$ , respectively. Due to this representation, only the six initial value problems associated with the initial conditions have to be

actually treated as differential equation systems. All variational equations related to dynamical orbit parameters, however, may be reduced to definite integrals, which can be efficiently solved numerically, e.g., with a Gaussian quadrature technique [7].

### 2.3.2.2 Piecewise Constant Accelerations

Let us now develop the mathematical background for estimating  $m$  constant accelerations  $A_i$  in the predetermined direction  $\mathbf{e}(t)$  for  $t_{i-1} \leq t < t_i$ ,  $i = 1, \dots, m$ . The contribution of this parameter  $P_i = A_i$  to  $\mathbf{f}_p$  in (2.14) is of the form  $A_i \cdot \mathbf{e}(t)$  for  $t_{i-1} \leq t < t_i$ . The corresponding variational equation reads as

$$\ddot{\mathbf{z}}_{A_i} = \mathbf{A}_0 \cdot \mathbf{z}_{A_i} + \mathbf{A}_1 \cdot \dot{\mathbf{z}}_{A_i} + \begin{cases} \mathbf{e}(t) ; & t_{i-1} \leq t < t_i \\ \mathbf{0} ; & \text{otherwise} \end{cases} . \quad (2.26)$$

The variational equation (2.26) may be easily solved thanks to the general mathematical properties of variational equations as developed in Sect. 2.3.2.1. Equation (2.25) reads for the special case of a piecewise constant acceleration as

$$\alpha_{A_i}(t) \doteq \int_{t_0}^t \mathbf{Z}^{-1}(t') \cdot \mathbf{h}_{A_i}(t') \cdot dt' = \int_{t_{i-1}}^{t^*} \mathbf{Z}^{-1}(t') \cdot \mathbf{h}_{A_i}(t') \cdot dt' , \quad (2.27)$$

where the upper integration limit is given by

$$t^* \doteq \begin{cases} t_{i-1} ; & t < t_{i-1} \\ t & ; t_{i-1} \leq t < t_i \\ t_i & ; t \geq t_i \end{cases} . \quad (2.28)$$

The solution  $\mathbf{z}_{A_i}(t)$  and its first time derivative for the parameter  $A_i$  follow from (2.24), and may be written as

$$\mathbf{z}_{A_i}^{(k)}(t) = \begin{cases} \mathbf{0} & ; t < t_{i-1} \\ \sum_{j=1}^6 \alpha_{O_j A_i}(t) \cdot \mathbf{z}_{O_j}^{(k)}(t) & ; t_{i-1} \leq t < t_i \\ \sum_{j=1}^6 \alpha_{O_j A_i}(t_i) \cdot \mathbf{z}_{O_j}^{(k)}(t) & ; t \geq t_i \end{cases} . \quad (2.29)$$

Note that  $\mathbf{z}_{A_i}(t)$  is a once (continuously) differentiable function of time for the entire arc. The non-zero coefficients  $\alpha_{O_j A_i}(t)$  are constant in time for the case  $t \geq t_i$ . This implies that a change in the parameter  $A_i$  does not only affect the orbit in the interval  $[t_{i-1}, t_i)$  where it is active, but it affects all positions (and velocities) for  $t \geq t_{i-1}$  as well. For a detailed discussion of an efficient solution strategy, the reader is referred to [64].

### 2.3.2.3 Pulses

Let us briefly mention the special case of instantaneous velocity changes  $V_i$  at times  $t_i$  in predetermined directions  $\mathbf{e}(t_i)$ , and outline how it fits into the formalism presented so far. The contribution of this parameter  $P_i = V_i$  to  $\mathbf{f}_p$  in (2.14) may formally be written as  $V_i \cdot \delta(t - t_i) \cdot \mathbf{e}(t)$ , where  $\delta(t)$  represents Dirac's delta function. The corresponding variational equation reads as

$$\ddot{\mathbf{z}}_{V_i} = \mathbf{A}_0 \cdot \mathbf{z}_{V_i} + \mathbf{A}_1 \cdot \dot{\mathbf{z}}_{V_i} + \delta(t - t_i) \cdot \mathbf{e}(t) . \quad (2.30)$$

Using the notation from Sect. 2.3.2.1, but identifying  $\mathbf{h}_{V_i}$  with  $\mathbf{h}_{A_i}$  in (2.27), the definite integral (2.27) may be simplified for  $t \geq t_i$  as

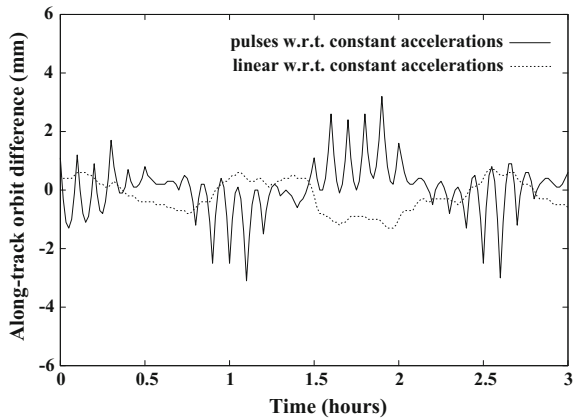
$$\alpha_{V_i}(t) \doteq \int_{t_0}^t \delta(t' - t_i) \cdot \mathbf{Z}^{-1}(t') \cdot \mathbf{h}_{V_i}(t') \cdot dt' = \mathbf{Z}^{-1}(t_i) \cdot \mathbf{h}_{V_i}(t_i) \doteq \beta_{V_i} . \quad (2.31)$$

Obviously,  $\alpha_{O_j V_i}(t)$  is zero for  $t < t_i$  and non-zero but constant for  $t \geq t_i$ . Therefore, the partial derivatives  $\mathbf{z}_{V_i}(t)$  may be written as a linear combination of only the six partial derivatives  $\mathbf{z}_{O_j}(t)$  of the a priori orbit w.r.t. the parameters defining the initial conditions at time  $t_0$ . The parametrization yields a continuous position vector  $\mathbf{r}(t)$  but, as opposed to the parametrization from Sect. 2.3.2.2, a discontinuous velocity vector  $\dot{\mathbf{r}}(t)$  of the improved orbit at the pulse epoch  $t_i$ . This parametrization may be viewed as a special case of the short-arc representation (see Sect. 2.3.2.5) of the entire arc, where the individual short-arcs are forced to be continuous at the arc boundaries.

### 2.3.2.4 Comparison Between Different Empirical Parametrizations

Fig. 2.10 shows a zoom of along-track differences between a 6 min pulse-based orbit with respect to an orbit which is based on 6 min piecewise constant accelerations. In

**Fig. 2.10** Along-track differences between a CHAMP orbit based on piecewise constant accelerations and orbits based on pulses and piecewise linear accelerations, respectively. Figure from [64]



addition, the differences between an orbit based on 6 min piecewise linear accelerations and the orbit based on 6 min piecewise constant accelerations is shown. The scale of Fig. 2.10 indicates that the differences induced by the different kinds of pseudo-stochastic orbit models are very small, provided that the subinterval length of the underlying parameters are not too long and that the a priori standard deviations are chosen appropriately. Figure 2.10 illustrates that from the point of view of orbit (position) modeling there is no significant gain to be expected when using more refined pseudo-stochastic parameters, e.g., piecewise linear accelerations instead of piecewise constant accelerations. Even the differences between the pulse and the acceleration solution are very small, although the effect of the instantaneous velocity changes can be well observed as sharp peaks at the pulse epochs every 6 min. Figure 2.10 gives one important reason for selecting piecewise constant accelerations as empirical parameters: they avoid obviously ‘unphysical’ phenomena in the orbits, but are easier to use than more sophisticated parametrizations such as piecewise linear accelerations.

### 2.3.2.5 Relation to Alternative Parametrizations

The short-arc parametrization represents the solution within each subinterval by a new set of six initial osculating elements, or, alternatively, by two boundary-value positions [97]. The resulting trajectory is thus characterized by a discontinuous velocity vector and a discontinuous position vector as well. It is not only possible to obtain such a trajectory by splitting the original orbital arc into several short-arcs by setting up new initial conditions at the beginning of each short-arc, but in the context of the methods discussed here to solve for one set of initial osculating elements and for instantaneous velocity changes  $V_i$  (see Sect. 2.3.2.3) in conjunction with instantaneous position changes  $X_i$  at times  $t_i$  in predetermined directions  $\mathbf{e}(t_i)$ . Using the notation from Sect. 2.3.2.2, but identifying  $\mathbf{h}_{X_i}$  with  $(\mathbf{e}^T(t_i), \mathbf{0}^T)$ , the coefficients of the partial derivatives  $\mathbf{z}_{X_i}(t)$  may be obtained in close analogy to Sect. 2.3.2.3 by

$$\alpha_{X_i}(t) \doteq \int_{t_0}^t \delta(t' - t_i) \cdot \mathbf{Z}^{-1}(t') \cdot \mathbf{h}_{X_i}(t') \cdot dt' = \mathbf{Z}^{-1}(t_i) \cdot \mathbf{h}_{X_i}(t_i) \doteq \beta_{X_i} \quad (2.32)$$

for  $t \geq t_i$ .

For the sake of completeness and clarity, the two linear systems of algebraic equations to be solved for the coefficients  $\alpha_{O_j X_i}(t_i)$  and  $\alpha_{O_j V_i}(t_i)$  of the partial derivatives  $\mathbf{z}_{X_i}(t)$  and  $\mathbf{z}_{V_i}(t)$ , respectively, may be explicitly written as



$$\begin{aligned}
\sum_{j=1}^6 \beta_{O_j X_i} \cdot \mathbf{z}_{O_j}(t_i) &= \mathbf{e}(t_i) \\
\sum_{j=1}^6 \beta_{O_j X_i} \cdot \dot{\mathbf{z}}_{O_j}(t_i) &= \mathbf{0} \\
\sum_{j=1}^6 \beta_{O_j V_i} \cdot \mathbf{z}_{O_j}(t_i) &= \mathbf{0} \\
\sum_{j=1}^6 \beta_{O_j V_i} \cdot \dot{\mathbf{z}}_{O_j}(t_i) &= \mathbf{e}(t_i)
\end{aligned}
, \tag{2.33}$$

which shows that the parameter  $X_i$  is ‘allowed’ to change only the orbital position at time  $t_i$  in direction  $\mathbf{e}(t_i)$ , but not the orbital velocity at time  $t_i$ . The opposite statement is valid for the parameter  $V_i$ .

The advantage of this alternative formulation is that the original arclength remains formally unchanged, i.e., it is easily possible to solve for deterministic orbit parameters still referring to the original arclength. This might matter if the deterministic orbit parameters are identified with geopotential coefficients. Instead of saving many (large) normal equation systems referring to the short arclength, a reduced number of normal equation systems may be generated, e.g., on a daily basis. For a discussion of further generalizations, e.g., to piecewise once-per-revolution periodic accelerations as they are also widely used for orbit determination, e.g., in the context of the lunar gravity mission GRAIL [92], we refer to [64].

### 2.3.3 Parameter Estimation

Classical least-squares adjustment (batch least-squares adjustment) is the mathematical method used in this chapter to outline precise orbit determination using precise satellite tracking data. A short overview of the most important formulas is therefore provided in the following subsection. We refer to Chap. 1 for a detailed introduction to parameter estimation techniques. For a discussion of other parameter estimation algorithms in the context of orbit determination, e.g., sequential estimators, we refer to, e.g., [141].

#### 2.3.3.1 Recapitulation of Least-Squares Adjustment

Let us assume that each observation may be expressed as a function of the parameters of a given mathematical model. Based on the model function  $\mathbf{F}$ , we may write the system of observation equations in the presence of observation errors as

$$\mathbf{L}' + \boldsymbol{\varepsilon} = \mathbf{F}(\mathbf{X}) . \tag{2.34}$$

If  $\mathbf{F}$  is a non-linear function of the parameters, it is linearized by

$$\mathbf{L}' + \boldsymbol{\varepsilon} = \mathbf{F}(\mathbf{X}_0) + \mathbf{A} \mathbf{x} , \quad (2.35)$$

with the column arrays  $\mathbf{L}'$  of the actual observations,  $\boldsymbol{\varepsilon}$  of the observation corrections (or residuals).  $\bar{\mathbf{L}} = \mathbf{L}' + \boldsymbol{\varepsilon}$  is the array of the adjusted observations,  $\mathbf{X} = \mathbf{X}_0 + \mathbf{x}$  the array of the adjusted model parameters,  $\mathbf{X}_0$  the array of the approximate (or a priori) model parameters,  $\mathbf{x}$  the array of the model parameter corrections w.r.t.  $\mathbf{X}_0$  (solution vector), and  $\mathbf{A}$ , which denotes the first design (or Jacobian) matrix. The first design matrix is defined by

$$\mathbf{A} \doteq \left. \frac{\partial \mathbf{F}(\mathbf{X})}{\partial \mathbf{X}} \right|_{\mathbf{X}=\mathbf{X}_0} \quad (2.36)$$

Rearranging the linearized observation equations yields

$$\boldsymbol{\varepsilon} = \mathbf{A} \mathbf{x} - (\mathbf{L}' - \mathbf{F}(\mathbf{X}_0)) = \mathbf{A} \mathbf{x} - \mathbf{l} , \quad (2.37)$$

where the term  $\mathbf{l} \doteq \mathbf{L}' - \mathbf{F}(\mathbf{X}_0)$  is often referred to as ‘observed-minus-computed’ (O–C).

The observation errors are characterized by a stochastic model, which in turn is described by the weight matrix of the observations

$$\mathbf{P} = \mathbf{Q}_{\parallel}^{-1} = \sigma_0^2 \mathbf{C}_{\parallel}^{-1} , \quad (2.38)$$

where  $\mathbf{Q}_{\parallel}$  is the cofactor matrix of the observations,  $\sigma_0$  is the a priori standard deviation of unit weight, and  $\mathbf{C}_{\parallel}$  is the covariance matrix of the observations. Note that the weight matrix  $\mathbf{P}$  is diagonal, if the observations are uncorrelated. In this case, the diagonal elements are given by  $P_{ll} = \sigma_0^2 / \sigma_l^2$ , where  $\sigma_l^2$  is the a priori variance of the corresponding observation.

In least-squares adjustment the solution of the observation equations (2.37) is obtained by minimizing the quadratic form  $\boldsymbol{\varepsilon}^T \mathbf{P} \boldsymbol{\varepsilon}$ . The underlying variation problem can be solved by Lagrange multipliers, which yield the normal equation system

$$(\mathbf{A}^T \mathbf{P} \mathbf{A}) \mathbf{x} - \mathbf{A}^T \mathbf{P} \mathbf{l} = \mathbf{N} \mathbf{x} - \mathbf{b} = \mathbf{0} , \quad (2.39)$$

where  $\mathbf{N} \doteq \mathbf{A}^T \mathbf{P} \mathbf{A}$  is the normal equation matrix and  $\mathbf{b} \doteq \mathbf{A}^T \mathbf{P} \mathbf{l}$  is the right-hand side of the normal equation system.  $\mathbf{N}$  is by definition a quadratic and symmetric matrix. If it is regular, the solution vector follows as

$$\mathbf{x} = (\mathbf{A}^T \mathbf{P} \mathbf{A})^{-1} \mathbf{A}^T \mathbf{P} \mathbf{l} = \mathbf{N}^{-1} \mathbf{b} , \quad (2.40)$$

where  $\mathbf{N}^{-1}$  is the inverse normal equation matrix. The estimated (a posteriori) standard deviation of unit weight is computed as

$$m_0 = \sqrt{\frac{\boldsymbol{\varepsilon}^T \mathbf{P} \boldsymbol{\varepsilon}}{f}} \quad (2.41)$$

for  $f > 0$ , where  $f \doteq n - u$  is the degree of freedom of the least-squares adjustment,  $n$  is the number of observations, and  $u$  is the number of adjusted model parameters. Note that the quadratic form (sum of the weighted residual squares) may be computed either using (2.37), which makes it necessary to evaluate the first design matrix  $\mathbf{A}$ , or, alternatively, by the more efficient but numerically less stable formula

$$\boldsymbol{\varepsilon}^T \mathbf{P} \boldsymbol{\varepsilon} = \mathbf{l}^T \mathbf{P} \mathbf{l} - \mathbf{x}^T \mathbf{b} . \quad (2.42)$$

The covariance matrix of the adjusted model parameters is given by

$$\mathbf{C}_{\mathbf{xx}} = m_0^2 \mathbf{Q}_{\mathbf{xx}} = m_0^2 \mathbf{N}^{-1} , \quad (2.43)$$

where  $\mathbf{Q}_{\mathbf{xx}}$  is the cofactor matrix of the adjusted model parameters. The (a posteriori) standard deviations of the adjusted model parameters are given by

$$m_x = \sqrt{C_{xx}} = m_0 \sqrt{Q_{xx}} , \quad (2.44)$$

where  $C_{xx}$  and  $Q_{xx}$  are diagonal elements of the covariance and cofactor matrices, respectively.

### Parameter Pre-elimination

The parameter pre-elimination technique is useful to handle a large number of model parameters efficiently, e.g., epoch-specific receiver clock offsets in case of GNSS data processing. Let us subdivide the system of normal equations (2.39) into two parts

$$\begin{bmatrix} \mathbf{N}_{11} & \mathbf{N}_{12} \\ \mathbf{N}_{21} & \mathbf{N}_{22} \end{bmatrix} \cdot \begin{bmatrix} \mathbf{x}_1 \\ \mathbf{x}_2 \end{bmatrix} = \begin{bmatrix} \mathbf{b}_1 \\ \mathbf{b}_2 \end{bmatrix} \quad (2.45)$$

and assume that we are not interested in the actual values of the solution sub-vector  $\mathbf{x}_2$ . In this case, we may reduce the normal equation system (2.45) by pre-eliminating the model parameters  $\mathbf{x}_2$ , which yields the modified system of normal equations as

$$\mathbf{N}_{11}^* \mathbf{x}_1 = \mathbf{b}_1^* , \quad (2.46)$$

where  $\mathbf{N}_{11}^* = \mathbf{N}_{11} - \mathbf{N}_{12} \mathbf{N}_{22}^{-1} \mathbf{N}_{21}$  is the normal equation matrix of the model parameters  $\mathbf{x}_1$  and  $\mathbf{b}_1^* = \mathbf{b}_1 - \mathbf{N}_{12} \mathbf{N}_{22}^{-1} \mathbf{b}_2$  is the corresponding right-hand side of the normal equation system. The pre-eliminated model parameters  $\mathbf{x}_2$  are correctly taken into account in the normal equation system (2.46) although their estimates are (without a dedicated back-substitution process) not available. One must be aware, however, that the parameter pre-elimination step cannot be performed at any arbitrary time;

it can be performed only if additional observations do no longer contribute directly to the elements related to the solution sub-vector  $\mathbf{x}_2$  of the normal equation system (2.45).

### Parameter Constraining

It is common practice to constrain selected model parameters to their a priori values ('absolute constraints') or to other parameters ('relative constraints'). This may be done to suppress large excursions of weakly determined model parameters from their a priori values or from neighboring parameter values. The technique is often applied to pseudo-stochastic orbit parameters in the context of LEO orbit determination. One must be aware, however, that a priori information is introduced into the system of normal equations through this process, which may or may not be desired for certain applications. Alternatively, parameters may be truly constrained to zero also in an iterative least-squares adjustment, which requires a transformation of the a priori parameter values. For an overview of advanced parameter modifications techniques on the normal equation level, we refer to [21]. Here, we just mention absolute constraining as the simplest and most often applied form of parameter constraining.

Parameter constraints may be introduced by artificial observations with a user-specified variance  $\sigma_{abs}^2$ . These observations have to be appended to the system of observation equations (2.35). If the change with respect to the a priori value is used as the actual parameter in the artificial observation equation, the weight

$$W = \frac{\sigma_0^2}{\sigma_{abs}^2} \quad (2.47)$$

has to be only added to the corresponding diagonal element of the normal equation matrix  $N$ , because the value O-C is zero in this special case. Observe that the degree of freedom has to be incremented by 1, as well.

#### 2.3.3.2 Partial Derivatives W.r.t. Orbit Parameters

In order to compute the partial derivatives (2.36) related to the  $r$ -th observation and the orbit parameter  $P_i$  it is advantageous to express the elements of the first design matrix (2.36) with the functions  $\mathbf{z}_{P_i}$  defined by (2.21)

$$\frac{\partial F_r(\mathbf{X})}{\partial P_i} = (\nabla F_r(\mathbf{X}))^T \cdot \mathbf{z}_{P_i} , \quad (2.48)$$

where  $F_r$  denotes the  $r$ -th component of the model function  $\mathbf{F}$ . Its gradient is given by

$$(\nabla F_r(\mathbf{X}))^T = \left( \frac{\partial F_r(\mathbf{X})}{\partial r_{0,1}} \quad \frac{\partial F_r(\mathbf{X})}{\partial r_{0,2}} \quad \frac{\partial F_r(\mathbf{X})}{\partial r_{0,3}} \right) . \quad (2.49)$$

Slightly more complicated relations (2.48) result if the observations depend not only on the geocentric position vector, but also on the velocity vector, or if they refer to more than one epoch. Equation (2.48) shows that only the gradient depends on the type of the observations. The functions  $\mathbf{z}_{P_i}$ , however, are independent of the observation type, which nicely separates the observation-specific (geometric) part from the dynamic part.

### 2.3.3.3 Structure of Normal Equations Related to Orbit Parameters

The structure of the orbit-related parts in the normal equation system may be exploited for setting-up an efficient solution strategy and to highlight the close relation of pseudo-stochastic orbit modeling techniques with filter strategies. Subsequently we derive the structure of a simplified orbit determination problem with initial conditions and pulses as the only parameters. More complicated scenarios are detailed in [64].

The observation equation (2.37) of observation number  $r$  of this orbit determination problem reads as

$$\varepsilon_r = \sum_{k=1}^6 \frac{\partial F_r}{\partial O_k} \cdot o_k + \sum_{m=1}^i \sum_{j=1}^3 \frac{\partial F_r}{\partial V_{m,j}} \cdot v_{m,j} - l_r, \quad (2.50)$$

where  $o_k$ ,  $k = 1, \dots, 6$  and  $v_{i,j}$ ,  $j = 1, \dots, 3$  denote the corrections to the six initial conditions and the three pulses at each epoch  $t_i$ ,  $i = 1, \dots, n-1$ , respectively; it is assumed that the observation time  $t_l$  is part of the subinterval  $[t_i, t_{i+1})$ . The relations (2.48) and (2.24) with the constant coefficients  $\beta_{O_k V_{m,j}}$  for pulses yield

$$\frac{\partial F_r}{\partial V_{m,j}} = (\nabla F_r)^T \cdot \mathbf{z}_{V_{m,j}} = (\nabla F_r)^T \cdot \sum_{k=1}^6 \beta_{O_k V_{m,j}} \cdot \mathbf{z}_{O_k}(t), \quad (2.51)$$

which is why the observation equation (2.50) can be rearranged as follows:

$$\varepsilon_r = \sum_{k=1}^6 (\nabla F_r)^T \cdot \mathbf{z}_{O_k} \cdot \left( o_k + \sum_{m=1}^i \sum_{j=1}^3 \beta_{O_k V_{m,j}} \cdot v_{m,j} \right) - l_r. \quad (2.52)$$

The term in parentheses has an important meaning. It does not represent the ‘initially’ solved for correction to the osculating element  $O_k$  at  $t_0$ , which would fully characterize the solution of this particular orbit determination problem in the subinterval  $[t_0, t_1)$ . Because a change in the initial osculating element  $O_k$  induced by a change in the pulse  $V_{i,j}$  can be computed as

$$\Delta O_k = \frac{\partial O_k}{\partial V_{i,j}} \cdot \Delta V_{i,j} = \beta_{O_k V_{i,j}} \cdot \Delta V_{i,j}, \quad (2.53)$$

the term in in Eq. (2.52) represents the correction  $o_{i,k}$  to a different initial osculating element  $O_{i,k}$  at  $t_0$  which fully characterizes the solution in the subinterval  $[t_i, t_{i+1})$  after the occurrence of the first 3  $i$  pulses. Equation (2.52) illustrates that orbit determination based on pulses may also be understood as a special case of the short-arc parametrization from Sect. 2.3.2.5 when asking for continuity at the short-arc boundaries. The properties of the newly defined osculating elements  $O_{i,k}$  at  $t_0$  will be exploited in Sect. 2.3.3.4. As the pulse epochs divide the orbital arc into  $n$  subintervals, it is advisable to write all  $n_{o_i}$  observation equations of the subinterval  $I_i = [t_i, t_{i+1})$  in a matrix notation

$$\boldsymbol{\varepsilon}_i = \mathbf{A}_i \mathbf{o} + \mathbf{A}_i \sum_{m=1}^i \mathbf{B}_m \mathbf{v}_m - \mathbf{l}_i, \quad (2.54)$$

with the column arrays  $\boldsymbol{\varepsilon}_i$  of the residuals of subinterval  $I_i$ ,  $\mathbf{l}_i$  of the terms O–C of subinterval  $I_i$ ,  $\mathbf{o}$  of the corrections to the initial osculating elements, and  $\mathbf{v}_i$  of the pulse corrections at epoch  $t_i$ . The matrix  $\mathbf{A}_i$  denotes the  $n_{o_i} \times 6$  first design matrix of the subinterval  $I_i$  related to the six initial osculating elements and  $\mathbf{B}_m$  denotes the  $6 \times 3$  coefficient matrix defined by  $B_{m[k;j]} \doteq \beta_{O_k} v_{m,j}$ .

Taking the observation equations of all subintervals  $I_i$ ,  $i = 0, \dots, n-1$  into account, the complete system of normal equations (2.39) reads in the above matrix notation as

$$\begin{bmatrix} \mathbf{N} & \sum_{i=1}^{n-1} \mathbf{N}_i \mathbf{B}_1 & \cdots & \sum_{i=n-1}^{n-1} \mathbf{N}_i \mathbf{B}_{n-1} \\ \cdot & \mathbf{B}_1^T \sum_{i=1}^{n-1} \mathbf{N}_i \mathbf{B}_1 & \cdots & \mathbf{B}_1^T \sum_{i=n-1}^{n-1} \mathbf{N}_i \mathbf{B}_{n-1} \\ \cdot & \cdot & \ddots & \vdots \\ \cdot & \cdot & \cdot & \mathbf{B}_{n-1}^T \sum_{i=n-1}^{n-1} \mathbf{N}_i \mathbf{B}_{n-1} \end{bmatrix} \cdot \begin{bmatrix} \mathbf{o} \\ \mathbf{v}_1 \\ \vdots \\ \mathbf{v}_{n-1} \end{bmatrix} = \begin{bmatrix} \mathbf{A}^T \mathbf{P} \mathbf{l} \\ \mathbf{B}_1^T \sum_{i=1}^{n-1} \mathbf{A}_i^T \mathbf{P}_i \mathbf{l}_i \\ \vdots \\ \mathbf{B}_{n-1}^T \sum_{i=n-1}^{n-1} \mathbf{A}_i^T \mathbf{P}_i \mathbf{l}_i \end{bmatrix}, \quad (2.55)$$

where  $\mathbf{N}_i \doteq \mathbf{A}_i^T \mathbf{P}_i \mathbf{A}_i$  is the part associated with the observation interval  $I_i$  of the normal equation matrix related to the six initial osculating elements. In analogy,  $\mathbf{A}_i^T \mathbf{P}_i \mathbf{l}_i$  is the contribution of the same subinterval to the right-hand side of the normal equation system related to the six initial osculating elements. The abbreviations

$$\mathbf{N} = \sum_{i=0}^{n-1} \mathbf{A}_i^T \mathbf{P}_i \mathbf{A}_i \quad \text{and} \quad \mathbf{A}^T \mathbf{P} \mathbf{l} = \sum_{i=0}^{n-1} \mathbf{A}_i^T \mathbf{P}_i \mathbf{l}_i \quad (2.56)$$

are the normal equation matrix and the right-hand side of the normal equation system of the deterministic problem without any pulses, respectively. Obviously, the contributions  $\mathbf{N}_i$  and  $\mathbf{A}_i^T \mathbf{P}_i \mathbf{l}_i$ ,  $i = 0, \dots, n-1$  do not only form the complete system of normal equations for dynamic POD according to Eq. (2.56), they are together with

the matrices  $\mathbf{B}_i$  also the building blocks of the complete system of normal equations (2.55) for reduced-dynamic POD based on pulses.

Equation (2.55) shows that the normal equation matrix has a simple structure. Unfortunately, it is not possible to apply the parameter pre-elimination technique (see Sect. 2.3.3.1) to any of the pseudo-stochastic parameters before the very last observation is incorporated into the system of normal equations. This can be seen from the upper summation limits in (2.55), which all include all subintervals up to the very last one. An efficient solution strategy, which is closely related to filter algorithms, may, however, be found and will be outlined in the next section.

### 2.3.3.4 Relation to Filter Solutions

Equation (2.52) implicitly introduced the transformation

$$\mathbf{o}_i \doteq \mathbf{o} + \sum_{m=1}^i \mathbf{B}_m \mathbf{v}_m \quad (2.57)$$

between the ‘initially’ solved for corrections  $\mathbf{o}$  to the a priori values of the initial osculating elements  $\mathbf{O}$  at  $t_0$  (subsequently denoted as  $\mathbf{o}_0$ ) and the corrections  $\mathbf{o}_i$  to the a priori values of the initial osculating elements  $\mathbf{O}_i$  at  $t_0$  which define the solution in the subinterval  $[t_i, t_{i+1})$ . For the following deliberations, it is convenient to define the transformation (2.57) recursively, and in reverse order as

$$\begin{aligned} \mathbf{o}_0 &\doteq \mathbf{o} \\ \mathbf{o}_{i-1} &\doteq \mathbf{o}_i - \mathbf{B}_i \mathbf{v}_i = (\mathbf{I}_6 - \mathbf{B}_i) \cdot \begin{bmatrix} \mathbf{o}_i \\ \mathbf{v}_i \end{bmatrix}; \quad i \geq 1 \end{aligned} \quad (2.58)$$

where  $\mathbf{I}_6$  denotes the identity matrix of dimension 6.

First, we consider the system of normal equations in the presence of initial conditions and pulses in its initial stages during the collection of the GPS observations. Let us assume that we already have incorporated all observations for times  $t_l \leq t_i$  and that the system may be written in a reduced form as

$$\bar{\mathbf{N}}_{i-1} \mathbf{o}_{i-1} = \bar{\mathbf{b}}_{i-1}. \quad (2.59)$$

The normal equation matrix  $\bar{\mathbf{N}}_{i-1}$  and the right-hand side  $\bar{\mathbf{b}}_{i-1}$  of the normal equation system (2.59) may be computed from the contributions to the normal equation system of the deterministic problem for the observation times  $t_l \leq t_i$ , i.e., from  $\mathbf{N}_l$  and  $\mathbf{b}_l$ ,  $l = 0, \dots, i-1$ , as

$$\begin{aligned}
\bar{\mathbf{N}}_0 &\doteq \mathbf{N}_0 \\
\bar{\mathbf{b}}_0 &\doteq \mathbf{b}_0
\end{aligned}
; i = 1$$

$$\begin{aligned}
\bar{\mathbf{N}}_{i-1} &\doteq \bar{\mathbf{N}}_{i-2}^* + \mathbf{N}_{i-1} \\
\bar{\mathbf{b}}_{i-1} &\doteq \bar{\mathbf{b}}_{i-2}^* + \mathbf{b}_{i-1}
\end{aligned}
; i \geq 2$$
(2.60)

with  $\bar{\mathbf{N}}_{i-2}^*$  and  $\bar{\mathbf{b}}_{i-2}^*$  to be defined later by (2.63).

The normal equation system (2.59) may be expanded into a system in the unknowns  $\mathbf{o}_i$  and  $\mathbf{v}_i$  by replacing  $\mathbf{o}_{i-1}$  on the left-hand side with the transformation (2.58), and by multiplying both sides of the normal equation system (2.59) from the left with the matrix  $(\mathbf{I}_6 - \mathbf{B}_i)^T$ :

$$\begin{bmatrix} \bar{\mathbf{N}}_{i-1} & -\bar{\mathbf{N}}_{i-1} \mathbf{B}_i \\ -\mathbf{B}_i^T \bar{\mathbf{N}}_{i-1} & \mathbf{B}_i^T \bar{\mathbf{N}}_{i-1} \mathbf{B}_i \end{bmatrix} \cdot \begin{bmatrix} \mathbf{o}_i \\ \mathbf{v}_i \end{bmatrix} = \begin{bmatrix} \bar{\mathbf{b}}_{i-1} \\ -\mathbf{B}_i^T \bar{\mathbf{b}}_{i-1} \end{bmatrix}.$$
(2.61)

The system (2.61) is the key to a most efficient solution of the orbit determination problem. According to the observation equation (2.52), the observations contained in the subintervals  $I_i, I_{i+1}, \dots, I_{n-1}$  do not depend on the terms  $\mathbf{v}_i$  explicitly as their influence is already taken into account by the osculating elements  $\mathbf{o}_i$ . It is thus possible to apply the parameter pre-elimination technique (see Sect. 2.3.3.1) to the pseudo-stochastic parameters. The normal equation system reads after the pre-elimination as

$$\bar{\mathbf{N}}_{i-1}^* \mathbf{o}_i = \bar{\mathbf{b}}_{i-1}^*$$
(2.62)

with

$$\begin{aligned}
\bar{\mathbf{N}}_{i-1}^* &\doteq \bar{\mathbf{N}}_{i-1} - \bar{\mathbf{N}}_{i-1} \mathbf{B}_i (\mathbf{B}_i^T \bar{\mathbf{N}}_{i-1} \mathbf{B}_i)^{-1} \mathbf{B}_i^T \bar{\mathbf{N}}_{i-1} \\
\bar{\mathbf{b}}_{i-1}^* &\doteq \bar{\mathbf{b}}_{i-1} - \bar{\mathbf{N}}_{i-1} \mathbf{B}_i (\mathbf{B}_i^T \bar{\mathbf{N}}_{i-1} \mathbf{B}_i)^{-1} \mathbf{B}_i^T \bar{\mathbf{b}}_{i-1}
\end{aligned}$$
(2.63)

A priori weights of the pseudo-stochastic parameters (see Sect. 2.3.3.1), e.g., in the form of absolute constraints given by an identical weight matrix

$$\mathbf{W} = \sigma_0^2 \mathbf{C}_{\mathbf{v}\mathbf{v}}^{-1}$$
(2.64)

for all pulse epochs, have to be added prior to the pre-elimination to the sub-matrix  $\mathbf{B}_i^T \bar{\mathbf{N}}_{i-1} \mathbf{B}_i$  of the normal equation matrix in (2.61).

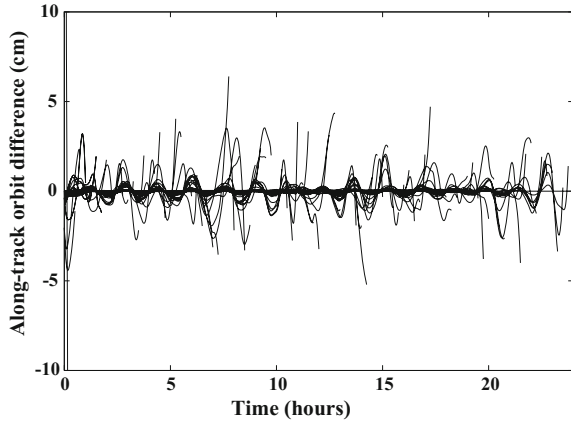
The procedure outlined by the Eqs. (2.59), (2.61), (2.62), and (2.60) has to be repeated until the very last observation of the subinterval  $I_{n-1}$  is incorporated into the reduced normal equation system. After completion of data collection, we may solve for the initial osculating element corrections  $\mathbf{o}_{n-1}$  of the last subinterval  $I_{n-1}$  by

$$\mathbf{o}_{n-1} = \bar{\mathbf{N}}_{n-1}^{-1} \bar{\mathbf{b}}_{n-1} = \mathbf{Q}_{o_{n-1}o_{n-1}} \bar{\mathbf{b}}_{n-1},$$
(2.65)

where  $\mathbf{Q}_{o_{n-1}o_{n-1}}$  is the cofactor matrix of the solved for corrections  $\mathbf{o}_{n-1}$ . Details of the algorithm, including the back-substitution process, are available in [64].



**Fig. 2.11** Along-track orbit differences between filter and least-squares reduced-dynamic solutions for CHAMP. Figure from [64]



The solution (2.65) shows that in principle there is no need to compute the ‘intermediary’ corrections  $\mathbf{o}_{i-1}$ ,  $i = 1, \dots, n - 1$  during data collection. They would actually represent the filter solutions based on all observations of the interval  $[t_0, t_i]$  and could be easily made available. It must be mentioned, however, that our definition of a ‘filter’ solution differs slightly from the usual terminology in the literature: it represents the least-squares solution of the considered orbit determination problem based on all observations from the very first epoch to the actually processed epoch. This implies that the orbit trajectory is still represented by pseudo-stochastic parameters, e.g., set up every  $n$ -th minute. A new filter solution is thus provided only every  $n$ -th minute as well, and not after each newly incorporated observation epoch. Only in the special case of pseudo-stochastic parameters set up at the observation sampling rate, the above algorithm will provide the same solutions as ‘classical’ filter solutions, where stochastic parameters are set up at every measurement epoch and the confidence in the dynamical modeling is controlled by process noise [105].

Figure 2.11 shows the along-track orbit differences between the least-squares solution for an orbit determination based on piecewise constant accelerations estimated over 15 min and different filter solutions. The filter trajectories were computed whenever a batch of 15 min of data had been collected, whereas the least-squares solution (last filter solution) was computed after data collection in the back-substitution process. It can be seen that large differences occur for the first 15 min which may be attributed to a weak determination of the orbit parameters from 15 min data only (filter initialization). The consistency between the individual filter solutions and the final least-squares solutions dramatically improves if longer data batches are processed, e.g., sub-millimeter differences at the beginning of the orbital arc are reached for a batch of 8 h. Figure 2.11 also shows, however, that the orbit solution is not very well constrained by the tracking data at the boundaries of the processed time span, which can be seen in this experiment at the right-ends of the individual filter solutions. The orbit consistency may be severely degraded by several centimeters. For this reason longer arcs are often processed than actually needed. When generating the GOCE precise science orbits in the frame of the GOCE High-level processing facility, 30 h

arcs of GPS carrier phase data were analyzed each day for orbit determination to minimize a degraded orbit quality at the boundaries of the central 24 h provided to the user community [16].

### **2.3.4 *Quality of GPS-Based LEO Orbit Determination***

A large number of LEO satellites with stringent accuracy requirements on orbit determination were equipped with high-quality dual-frequency GPS receivers in the last two decades. Examples are the altimetry satellites TOPEX/Poseidon, Jason-1 and -2 [44, 91, 101], the gravity missions CHAMP, GRACE, and GOCE [37, 121, 142], the Synthetic Aperture Radar (SAR) satellites TerraSAR-X and TanDEM-X [24, 88], the magnetic field mission Swarm [43], and the currently launched Sentinel satellites serving various purposes of Earth observation. For all these missions high-quality orbit solutions were/are generated by many research teams. Selected results and the associated publications are highlighted in the subsequent sections. For an overview of methodologies for orbit determination based on single-frequency GPS data, we refer to, e.g., [14].

The core products from the IGS [36], such as highly accurate GPS ephemerides, Earth rotation parameters, and GPS satellite clock corrections, are the backbone for precise orbit determination of LEO satellites. Especially GPS satellite clock corrections are indispensable for precise orbit determination when using undifferenced GPS data. Alternatively, double differences may be formed between two spaceborne receivers of formation flying satellites, or between a spaceborne and terrestrial receivers of the IGS ground tracking network to allow for a relative positioning of the LEO satellites [64]. Subsequently, however, we highlight results from GRACE and GOCE orbit determination which are based on undifferenced GPS data and the orbit and clock products from the Center for Orbit Determination in Europe (CODE), one of the global analysis centers of the IGS [28]. In view of the available sampling rates of usually 0.1–1 Hz of the GPS observations from spaceborne receivers, high-rate clock corrections are of crucial importance to avoid the interpolation errors of GPS satellite clock corrections over long intervals and to guarantee the best possible results for orbit determination [15].

#### **2.3.4.1 SLR Validation**

For LEO satellites equipped with a laser retro reflector array, independent SLR measurements collected by the tracking network of the International Laser Ranging Service (ILRS, [114]) may be used to compare the observed SLR ranges to the satellites with the computed ranges derived from the GPS-based reduced-dynamic or kinematic ephemerides. This allows for an absolute validation of the line-of-sight directions between the SLR tracking stations and the LEO satellites, i.e., it allows to directly assess the one-dimensional orbit accuracies in these directions. For high

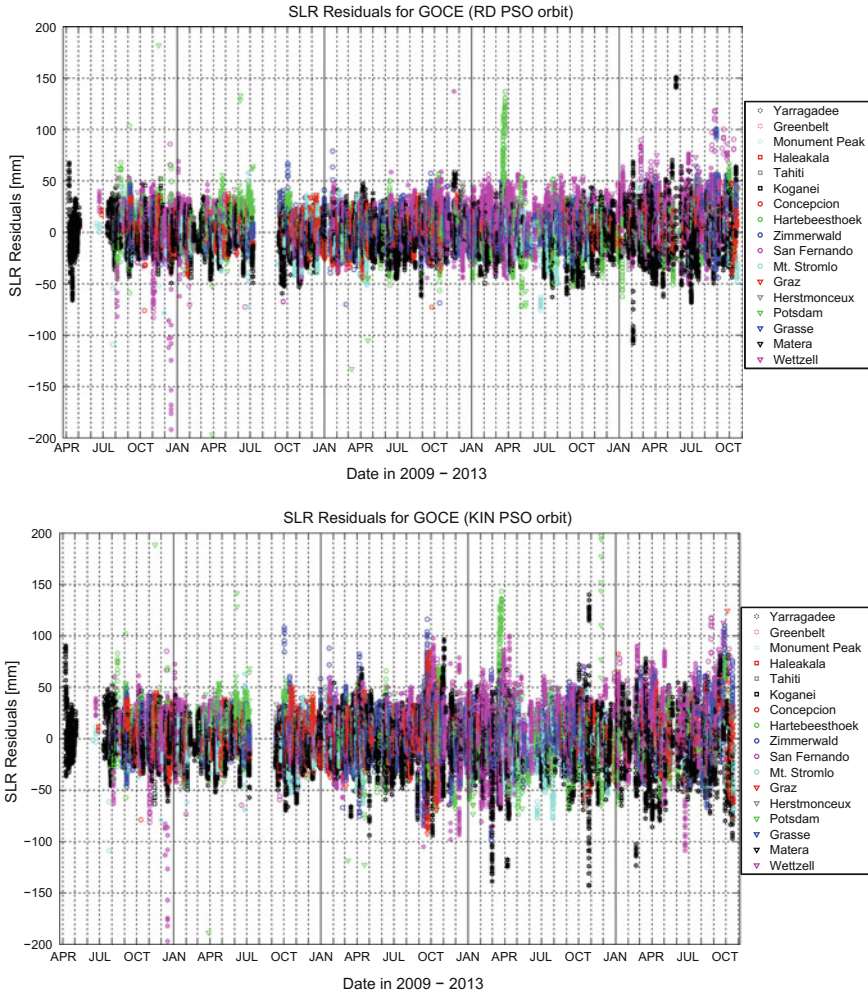


**Fig. 2.12** SLR validation of reduced-dynamic (*top*) and kinematic (*bottom*) GOCE precise science orbits. Figure from [18]

elevation passes the line-of-sight direction mainly corresponds to the radial direction of the co-rotating orbital frame. SLR data collected at low elevations, however, may also be used to recover along-track and cross-track orbital errors if the satellites are orbiting the Earth at sufficiently low altitudes. This became obvious for the extremely low orbital altitude of the GOCE satellite, where systematic orbital shifts in the cross-track direction, caused by unmodeled GPS antenna phase center variations, could be directly confirmed by SLR [17, 68]. Recently, systematic cross-track biases were quantified from SLR residuals data as a function of high-fidelity dynamic orbit models used for the TerraSAR-X satellite orbiting the Earth at a higher orbital altitude [48].

Figure 2.12 shows the SLR residuals of the reduced-dynamic and the kinematic orbits of the GOCE precise science orbits over the entire mission [18]. In order not to deteriorate the validation by single outliers, SLR residuals larger than 20 cm are excluded. The overall SLR RMS error of the reduced-dynamic orbits is 1.84 cm and impressively shows the quality of pseudo-stochastic orbit modeling techniques. A slightly worse but still excellent validation is obtained for the kinematic orbits with 2.42 cm. This is expected, because kinematic orbits are more sensitive to GPS data problems. Due to the large number of 12 channels of the GOCE onboard GPS receiver, the quality of the kinematic positions is outstanding. Current LEO satellites such as those from the Swarm mission, which are all equipped with 8-channel receivers, do not allow to generate kinematic orbits of the same quality [72]. Figure 2.12 shows, however, that the accuracy of both types of GOCE orbits is degrading towards the end of the mission. This is unexpected and was found to be related to problems in the GOCE GPS data [18, 71].

### 2.3.4.2 K-Band Validation

For the GRACE twin satellites which are following each other on the same orbit in a distance of about 200 km, an additional independent validation of the orbit quality may be performed. K-band measurements may be used to compare the orbit-derived distances between the two GRACE satellites with the biased ranges which are directly observed by the ultra-precise K-band ranging system [36]. Figure 2.13 (left) shows the daily K-band range standard deviation obtained from distances computed every 5 s between reduced-dynamic GRACE-A and -B orbit positions derived from zero-difference or double-difference GPS carrier phase data with empirical receiver antenna phase center variations (PCVs) taken into account or not. Figure 2.13 (left)

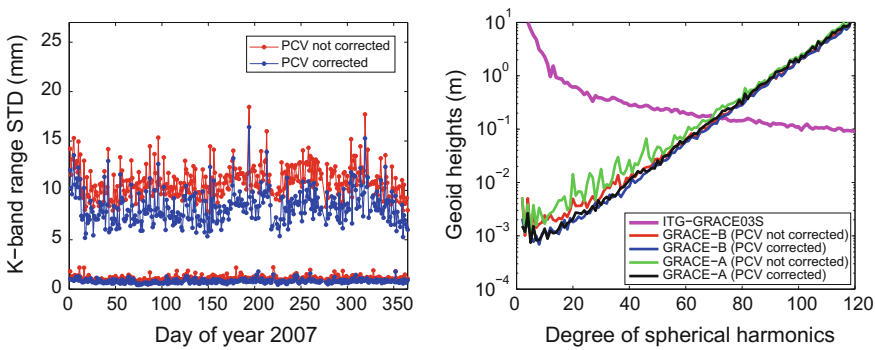


**Fig. 2.13** Impact of PCV modeling on daily standard deviations of K-band range residuals for distances between reduced-dynamic GRACE-A and GRACE-B orbits using undifferenced (*left, top curves*) or doubly-differenced GPS data with resolved carrier phase ambiguities (*left, bottom curves*) and on difference degree amplitudes of gravity field recoveries based on one year of kinematic GRACE orbits (*right*). Figures from [67]

shows that the relative orbit precision of GRACE reduced-dynamic orbit determination is about 1 cm when using zero-difference GPS carrier phase observations and about 1 mm when using double-difference GPS carrier phase observations with ambiguities fixed to their integer values [64]. In both cases the reduction of systematic carrier phase measurement errors, e.g., by empirical modeling of antenna phase center variations, is of crucial relevance to derive trajectories of highest quality [66]. The same statement holds for kinematic orbits, which are particularly sensitive to systematic carrier phase errors. Figure 2.13 (right) shows that unmodeled receiver PCVs may even propagate into gravity field solutions derived from kinematic GRACE positions in the frame of a generalized orbit determination problem (see next section). Further systematic carrier phase errors were identified in the frame of the GOCE and the Swarm missions and suspected to be related to the modeling of higher order ionosphere correction terms [18, 145]. They propagate via orbits into the gravity field estimation, as well [71, 72].

### 2.3.5 Generalized Orbit Determination

Based on a given a priori orbit  $\mathbf{r}_0(t)$  orbit improvement as introduced in Sect. 2.3.1.2 may be generalized by including a variety of different types of other than just arc-specific orbit parameters. Gravity field recovery may in particular be understood and treated as a generalized orbit improvement problem relying on the analysis of a large number of orbital arcs. In analogy to Sect. 2.3.1.2 the actual orbit  $\mathbf{r}(t)$  of an involved satellite may be expressed for each orbital arc as a truncated Taylor series with respect to the unknown orbit parameters  $O_i$  (arc-specific parameters) and, e.g., the unknown coefficients of the Earth's gravity field  $Q_i$  (global parameters) about the a priori orbit, which is represented by the a priori parameter values  $O_{0i}$  and  $Q_{0i}$ :

$$\mathbf{r}(t) = \mathbf{r}_0(t) + \sum_{i=1}^{n_o} \frac{\partial \mathbf{r}_0(t)}{\partial O_i} \cdot o_i + \sum_{i=1}^d \frac{\partial \mathbf{r}_0(t)}{\partial Q_i} \cdot q_i, \quad (2.66)$$

where  $o_i \doteq O_i - O_{0,i}$  denote the  $n_o$  corrections to be estimated for the arc-specific orbit parameters and  $q_i \doteq Q_i - Q_{0,i}$  the  $d$  corrections to the global coefficients of the Earth's gravity field.

Analogously, gravity field recovery from inter-satellite measurements, e.g., from K-band ranging between the two GRACE satellites, may be understood and treated as a generalized differential orbit improvement process, as well. The actual orbit difference  $\mathbf{r}_a(t) - \mathbf{r}_b(t)$  may be expressed as a truncated Taylor series with respect to the unknown parameters about the a priori orbit difference. The distinction needs to be made between  $n_{aO}$  parameters  $O_{ai}$  and  $n_{bO}$  parameters  $O_{bi}$ , which are specific to the orbital arcs of GRACE-A and -B, respectively, and  $d$  global parameters  $Q_i$ , which are common to both GRACE satellites such as the coefficients of the Earth's gravity field. The truncated Taylor series then reads as

$$\begin{aligned}
\mathbf{r}_a(t) - \mathbf{r}_b(t) = & \mathbf{r}_{a0}(t) - \mathbf{r}_{b0}(t) \\
& + \sum_{i=1}^{n_{aO}} \frac{\partial \mathbf{r}_{a0}(t)}{\partial O_{ai}} \cdot O_{ai} \\
& - \sum_{i=1}^{n_{bO}} \frac{\partial \mathbf{r}_{b0}(t)}{\partial O_{bi}} \cdot O_{bi} \\
& + \sum_{i=1}^d \left( \frac{\partial \mathbf{r}_{a0}(t)}{\partial Q_i} - \frac{\partial \mathbf{r}_{b0}(t)}{\partial Q_i} \right) \cdot q_i
\end{aligned} \tag{2.67}$$

The partial derivatives in Eqs. (2.66) and (2.67) are obtained by solving the corresponding variational equations as outlined in Sect. 2.3.2.1. Note that Eqs. (2.24) and (2.25) from Sect. 2.3.2.1 are valid for any orbit parameters, in particular for gravity field coefficients. The solution of the variational equations corresponding to gravity field parameters is thus reduced to numerical quadrature.

In order to set-up the observation equations, the partial derivatives of the a priori orbits need to be related to the observables, e.g., according to Sect. 2.3.3.2 for GPS data or by projecting the respective terms in Eq. (2.67) to the line-of-sight between GRACE-A and -B in the case of K-Band biased range observations. Special care is needed to not lose numerical precision related to orbit parameters in case of ultra-precise biased range observations and the resulting, very similar partials for the close formation of both satellites. The problem can be substantially mitigated by transforming the original orbital parameters of both satellites to the sum and the differences of the original orbital parameters [11]. In case of GPS data or kinematic positions used as pseudo-observations for a satellite trajectory, the observation equations may be written in matrix notation as

$$\boldsymbol{\varepsilon} = \mathbf{A}_o \mathbf{o} + \mathbf{A}_q \mathbf{q} - \mathbf{l}, \tag{2.68}$$

where  $\mathbf{o}$  contains all parameters defining the initial conditions, all satellite- and arc-specific dynamic parameters, and all pseudo-stochastic parameters,  $\mathbf{q}$  contains all common dynamic parameters such as the gravity field coefficients, and  $\mathbf{A}_o$  and  $\mathbf{A}_q$  are the first design matrices corresponding to the parameter arrays  $\mathbf{o}$  and  $\mathbf{q}$ . According to Eq. (2.39) the system of normal equations reads as

$$\begin{bmatrix} \mathbf{N}_{oo} & \mathbf{N}_{oq} \\ \mathbf{N}_{oq}^T & \mathbf{N}_{qq} \end{bmatrix} \cdot \begin{bmatrix} \mathbf{o} \\ \mathbf{q} \end{bmatrix} = \begin{bmatrix} \mathbf{b}_o \\ \mathbf{b}_q \end{bmatrix} \tag{2.69}$$

with  $\mathbf{N}_{oo} = \mathbf{A}_o^T \mathbf{P} \mathbf{A}_o$ ,  $\mathbf{N}_{oq} = \mathbf{A}_o^T \mathbf{P} \mathbf{A}_q$ ,  $\mathbf{N}_{qq} = \mathbf{A}_q^T \mathbf{P} \mathbf{A}_q$ , and  $\mathbf{b}_o = \mathbf{A}_o^T \mathbf{P} \mathbf{l}$ ,  $\mathbf{b}_q = \mathbf{A}_q^T \mathbf{P} \mathbf{l}$ . Similar NEQs may be also set-up for other observables such as K-Band, where orbital parameters of both satellites have to be included, however, in  $\mathbf{o}$ . The underlying normal equation matrices are therefore singular when trying to solve them from K-band data alone without the normal equation contributions from GPS. The normal equation contributions stemming from each observable may be super-imposed for each orbital arc by adopting measurement-specific weight factors, see

[10, 11]. Furthermore, the arc-specific parameters can be pre-eliminated according to Eq. (2.46), which yields the reduced system

$$(\mathbf{N}_{qq} - \mathbf{N}_{oq}^T \mathbf{N}_{oo}^{-1} \mathbf{N}_{oq}) \mathbf{q} = \mathbf{b}_q - \mathbf{N}_{oq}^T (\mathbf{N}_{oo}^{-1} \mathbf{b}_o) \quad (2.70)$$

The dimension of the resulting normal equation system is reduced by the number of arc-specific parameters  $\mathbf{o}$ , while the impact of these parameters is correctly taken into account when solving for the gravity field coefficients. To solve for these coefficients up to the desired resolution, normal equation systems stemming from a large number of arcs have to be accumulated to achieve the needed spatial coverage before the corrections to the a priori parameter values can be obtained by inversion of the accumulated normal equation system according to Eq. (2.40).

### 2.3.5.1 Gravity Field Determination from Kinematic Positions

Figure 2.14 shows the typical performance of static gravity field recoveries derived from different sets of kinematic positions of LEO satellites used as pseudo-observations to solve a generalized orbit determination problem as outlined above. Shown are square-roots of the degree difference variances of the GPS-only gravity field recoveries with respect to superior gravity field models based on dedicated measurements such as GRACE K-Band and GOCE gradiometer observations [98, 99]. The GPS-only solutions shown in Fig. 2.14 (left) are all based on different amounts of data. Only the solutions based on GOCE and GRACE-B kinematic positions are based on a rather similar time span such that a comparable quality may be expected for the low degree SH coefficients. For the determination of the higher degree coefficients, however, GOCE GPS data is significantly better suited than GRACE GPS data due to the lower orbital altitude, which is reflected by the smallest slope in Fig. 2.14

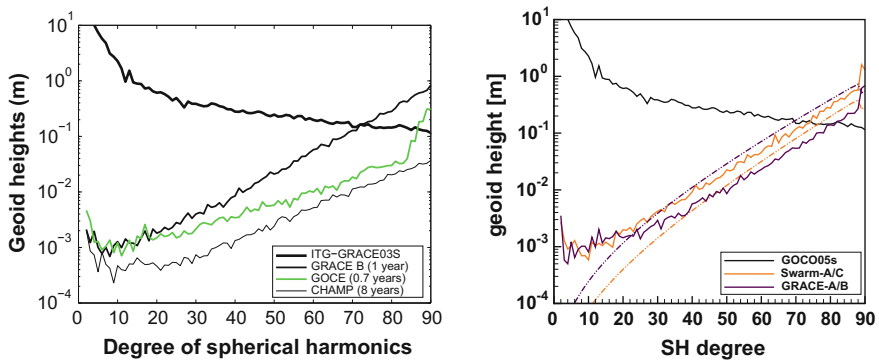


**Fig. 2.14** Square-roots of degree difference variances of gravity field recoveries from kinematic positions of GRACE-B, GOCE, and CHAMP (*left*) and GRACE-A, -B and Swarm-A, -C (*right*). Figures from [69, 72]



(left). The CHAMP solution is based on a significantly larger amount of data and therefore superior to the other solutions. Figure 2.14 (right) shows more recent and better comparable recoveries based on one year of GRACE-A and -B and Swarm-A and -C kinematic positions, respectively. Again Swarm is equally well suited to derive the long wavelength part of the Earth's gravity field as it is possible from GRACE GPS data. This is of relevance to bridge a potential gap between the GRACE mission and the GRACE Follow-On mission to continue the monitoring of the (long wavelength part) of the Earth's time-variable gravity field [40]. Encouraging results based on CHAMP, GRACE, GOCE, and Swarm GPS data have been reported by [71, 72, 158, 163]. For degrees above 20 in Fig. 2.14 (right), however, the GRACE solution outperforms the Swarm solution. This is only to a minor extent related to the higher orbital altitude of the Swarm satellites, as indicated by only a slightly larger slope of the Swarm formal errors, but mostly related to a more problematic quality of the Swarm GPS data [72].

### 2.3.5.2 Separation of Orbit and Gravity Field Determination

For didactic reasons we abandon in this section the processing scheme described in the previous section and fix the arc-specific parameters to previously determined values, while estimating the corrections to the gravity field parameters. This may be done by explicitly solving for the arc-specific parameters using the a priori force model and by consequently deleting them from the NEQ-system, instead of following the implicit and correct solution described by Eq. (2.70). This procedure implies that the sub-system

$$\mathbf{N}_{oo} \mathbf{o}' = \mathbf{b}_o \quad (2.71)$$

is solved independently from the remaining parts of Eq. (2.69) and that the parameters  $\mathbf{o}'$  are introduced in the following gravity recovery step as known. The remaining normal equation system

$$\mathbf{N}_{qq} \mathbf{q}' = \mathbf{b}_q - \mathbf{N}_{oq}^T \mathbf{o}' = \mathbf{b}_q - \mathbf{N}_{oq}^T (\mathbf{N}_{oo}^{-1} \mathbf{b}_o) \quad (2.72)$$

inevitably leads to solutions  $\mathbf{q}'$  for the gravity model parameters different from the solutions  $\mathbf{q}$  in Eq. (2.70). In the case of a separate solution of orbit and gravity field coefficients the orbit parameters  $\mathbf{o}'$  fully depend on the a priori gravity model and the correlations between orbit and gravity field parameters are ignored. As a consequence the estimated gravity field parameters  $\mathbf{q}'$  are biased, as well, towards the a priori gravity field. For details concerning the consequences of this approach, we refer to [103], where the impact on gravity field recovery is studied and where it is shown that the conditions  $\mathbf{N}_{oq} \mathbf{q} = \mathbf{0}$  used to separate orbit and gravity field determination (compare Eqs. (2.70) and (2.72)) are actually equivalent to a special regularization imposed on the gravity field coefficients resulting in recoveries biased towards the a priori gravity field.



### 2.3.5.3 Relation to the Acceleration Approach

Let us assume that the second derivatives of the position vector have been observed (in practice derived by numerical differentiation from kinematic positions). The observation equations for the accelerations referring to one particular epoch  $t_r$  follow from Eq. (2.68) by identifying the observations with kinematic positions and by taking the second time derivative as

$$\varepsilon_r = \sum_{k=1}^{n_0} \frac{\partial \ddot{\mathbf{r}}(t_r)}{\partial O_k} \cdot o_k + \sum_{k=1}^d \frac{\partial \ddot{\mathbf{r}}(t_r)}{\partial Q_k} \cdot q_k - \Delta \ddot{\mathbf{r}}_r, \quad (2.73)$$

where  $\Delta \ddot{\mathbf{r}}_r$  represents the observed minus the computed acceleration. The partial derivatives in the second sum may be replaced by the right-hand sides of the variational equations (2.22) as

$$\frac{\partial \ddot{\mathbf{r}}(t_r)}{\partial Q_k} = \frac{\partial \mathbf{f}(t_r)}{\partial \mathbf{r}(t_r)} \cdot \frac{\partial \mathbf{r}(t_r)}{\partial Q_k} + \frac{\partial \mathbf{f}(t_r)}{\partial \dot{\mathbf{r}}(t_r)} \cdot \frac{\partial \dot{\mathbf{r}}(t_r)}{\partial Q_k} + \frac{\partial \mathbf{f}(t_r)}{\partial Q_k}, \quad (2.74)$$

where use was made of Eq. (2.23). The observation equations used in the acceleration approach, e.g., [6], simply read as

$$\varepsilon_r = \sum_{k=1}^d \frac{\partial \mathbf{f}(t_r)}{\partial Q_k} \cdot q_k - \Delta \ddot{\mathbf{r}}_r. \quad (2.75)$$

From the point of view of orbit determination this implies that the following approximation was made:

$$\sum_{k=1}^{n_0} \frac{\partial \ddot{\mathbf{r}}(t_r)}{\partial O_k} \cdot o_k + \sum_{k=1}^d \left( \frac{\partial \mathbf{f}(t_r)}{\partial \mathbf{r}(t_r)} \cdot \frac{\partial \mathbf{r}(t_r)}{\partial Q_k} + \frac{\partial \mathbf{f}(t_r)}{\partial \dot{\mathbf{r}}(t_r)} \cdot \frac{\partial \dot{\mathbf{r}}(t_r)}{\partial Q_k} \right) = \mathbf{0}. \quad (2.76)$$

The acceleration method thus assumes that the changes in the second derivatives of the orbit caused by the estimated gravity field parameters  $q_k$  are counterbalanced by changes of the second derivatives of the orbit due to the changes in the arc-specific parameters  $o_k$ . The assumption is obviously met if the a priori orbit used to compute  $\Delta \ddot{\mathbf{r}}_r$  in the acceleration approach equals the estimated a posteriori orbit resulting from classical orbit determination. If this is not the case, the assumption cannot be met precisely. For further discussions and comparisons of the outlined orbit determination strategies with other approaches such as the short-arc approach, the reader is referred to [11].

## 2.4 Exercises



Data and files needed for the following exercises are available online at:  
<http://aiuws.unibe.ch/WEHeraeusAS2015/Chapter2-OrbitDetermination.zip>

### 1: Orbit determination using a least-squares solution and a filter solution

In this exercise a true orbit in the two-body problem is used, from which a number of pseudo-observations is created. Your main task is then to perform an orbit determination using a conventional least-squares solution and a filter solution. You will perform the task by completing the MATLAB skeleton file **ex1.m**. In this file, incomplete lines are commented out (by the character `%`) and marked with ‘TO BE COMPLETED’. The following MATLAB functions are available and can be used:

- **[*x v*] = ephem(GM,ele,tOsc,t)**: This function takes the gravity constant **GM**, a 6-element array **ele** containing the six Keplerian orbital elements,
  - **ele(1)**: semi-major axis,  $a$
  - **ele(2)**: numerical eccentricity,  $e$
  - **ele(3)**: inclination,  $i$
  - **ele(4)**: right ascension of ascending node,  $\Omega$
  - **ele(5)**: argument of perigee,  $\omega$
  - **ele(6)**: argument of latitude at osculating epoch,  $u_0$ ,
 the osculating epoch **tOsc** (set to zero in all exercises), and an arbitrary epoch **t**. It returns the vectors **x** and **v**, which contain the position and the velocity of the satellite (in the geocentric inertial frame) at epoch **t**. The formulas of the two-body problem are used for the orbit propagation.
- **ele = xyzele(GM,x,v,tOsc,t)**: This function is the inverse of the function **ephem**, i.e., it takes **GM**, an osculating epoch **tOsc** (set to zero in all exercises), an epoch **t** and the vectors **x** and **v**, containing position and velocity of the satellite at epoch **t**, and returns the array **ele** with the above six orbital elements.
- **[drdele dvdele] = rvpder(ini,GM,t,tOsc,ele)**: This function computes the partial derivatives of positions and velocities of a Keplerian orbit w.r.t. the Keplerian elements. It takes **GM**, the epoch **t** at which the partials shall be computed, the osculating epoch **tOsc** (set to zero in all exercises) and the Keplerian elements **ele**. The first argument **ini** is set to 1 in order to initialize the computation (on first call). The function returns the  $3 \times 6$  matrices **drdele** and **dvdele** which contain the partial derivatives.

At the beginning of the MATLAB skeleton file **ex1.m** the six Keplerian elements of an orbit of a two-body problem are defined (osculating epoch is 0):

- $a = 6800 \text{ km}$
- $e = 0.05$
- $i = 89^\circ$
- $\Omega = 130^\circ$

- $\omega = 30^\circ$
- $u_0 = 30^\circ$

These elements define the true orbit which shall be determined during this exercise. Using the function **ephem**, every 30 s the position vector of the satellite is computed (for a full day). A normally distributed noise is added to the positions, which are then stored in the matrix **psdObs** (rows: components, columns: epochs). These positions serve as pseudo-observations for the following orbit determination.

- For a first crude initial orbit determination, take the first **nObsIni = 10** observations of the day and fit a polynomial of degree **polDeg = 4** through each component separately by using the MATLAB command **polyfit**.<sup>1</sup> Use  $t - t_{Avg}$  as time argument of the polynomials, where  $t_{Avg}$  is the center of the initial observation period. Use these polynomials to compute the position and velocity vector of the satellite at time  $t_{Avg}$ . Use the function **xyzele** to find the corresponding orbital elements from these vectors. What are their values? These elements shall serve as a priori orbital elements for the orbit determination.<sup>2</sup>
- Compute and plot the differences of the a priori orbit (obtained from the a priori orbital elements computed in exercise 1a and the true orbit for all epochs of the day in the geocentric ( $x, y, z$ ) and in the local orbital (radial  $R$ , along-track  $S$ , cross-track  $C$ ) frame. In which component is the difference largest? Why?
- Perform a conventional least-squares solution of the orbit determination problem, i.e., solve for the six orbital elements. Use the pseudo-observations in **psdObs** with equal weighting and introduce the orbital elements computed in exercise 1a as a priori values. Perform the following steps:
  - Loop over all epochs. For each epoch:
    - Compute the satellite position using the function **ephem** and the a priori orbital elements.
    - Compute the ‘observed minus computed’ term.
    - Compute the first design matrix using the function **rvpder**.
    - Accumulate the normal equation system.
  - Solve the normal equation system<sup>3</sup> and compute the a posteriori standard deviation of unit weight.
  - Update the orbital elements.

What are the values of the updated orbital elements?

<sup>1</sup>Usage: **p = polyfit(x, y, n)**, where **p** are the coefficients of a polynomial  $p(x)$  of degree **n**, that is a best fit (in a least-squares sense) for the data in **y**. The coefficients in **p** are in descending powers, and the length of the array **p** is **n + 1**.

<sup>2</sup>Please notice that this way of initial orbit determination is not what is usually done; there are much more elaborate approaches which lead to more accurate initial orbits.

<sup>3</sup>You can solve the normal equation system by inverting the normal equation matrix (using the MATLAB command **inv**) and multiplying by the right hand side of the normal equation system. However, a faster and more robust way to solve a linear system is by using the command **mldivide** (matrix left division): **x = mldivide(A, b)** solves the linear system  $\mathbf{A} \cdot \mathbf{x} = \mathbf{b}$ . The abbreviation for **mldivide** is the backslash operator: **x = A\b**.

(d) Compute the residuals in two ways:

- Consider the linearized problem of the least-squares adjustment and calculate the residuals as they appear in the linearized observation equations.
- Take the updated orbital elements and propagate the orbit using the function **ephem**. For each epoch compute the differences between the propagated orbit and the observations.

Plot the  $z$ -component of the two kinds of residuals. Why are they different?

(e) Perform a filter solution of the orbit determination problem using the recursive filter formulas (see the online data) for the inverted normal equations. Use the pseudo-observations in **psdObs** with equal weighting and introduce the orbital elements computed in exercise 1a as a priori values. Perform the following steps:

- Loop over the first two epochs and initialize the filter:
  - Compute the satellite position using the function **ephem** and the a priori orbital elements.
  - Compute the ‘observed minus computed’ term.
  - Compute the first design matrix using the function **rvpder**.
  - Accumulate the normal equation system.
- Solve the normal equation system of the initialization.
- Loop over the remaining epochs and perform the filter steps:
  - Compute the satellite position using the function **ephem** and the a priori orbital elements.
  - Compute the ‘observed minus computed’ term.
  - Compute the first design matrix using the function **rvpder**.
  - Compute the resubstitution term as shown in the lecture slides (see the online data).
  - Compute the gain matrix as shown in the lecture slides (see the online data).
  - Update the solution vector. Store the solution vector at each filter step.

Plot the determined semi-major axis  $a$  for all filter steps. When does it converge?

Plot the  $x$ -component of the resubstitution term for each filter step.

(f) Implement the conventional least-squares adjustment into an iteration loop, where, at each step, you use the updated orbital elements from the previous step as a priori elements. Think about a reasonable stop criterion for the iteration loop. Compute and plot the linearized and true residuals after the last iteration.

## 2: Orbit determination with pseudo-stochastic pulses

Here, we use a ‘true’ orbit which was obtained by not only using the equations of motion of the two-body problem, but by additionally applying along-track (perturbation) accelerations in a numerical integration. From this orbit a number of pseudo-observations are created. Your main task is then to use these pseudo-observations to perform the orbit determination in the frame of the two-body problem, but by additionally solving for pseudo-stochastic pulses, which shall compensate the perturbing accelerations. You will again carry out a conventional least-squares adjustment and a filter approach.

You will perform the task by completing the MATLAB skeleton file **ex2.m**. The same MATLAB functions as in exercise 1 are used. At the beginning of the MATLAB skeleton file **ex2.m** the same six Keplerian elements as in exercise 1 are defined. Starting from the initial conditions defined by these elements, a perturbed orbit was created beforehand by numerical integration of the equations of motion by taking the 10 s piecewise constant along-track accelerations in the file **GRCA.ACC** into account. The positions and velocities resulting from the numerical integration were written in a 30 s sampling into the file **STOCH\_ORB** (column 1: time, columns 2-4: positions in geocentric inertial frame, columns 5-7: velocities). This file is read (using the MATLAB command **load**). Using the function **xyzele**, for each 30 s epoch a set of osculating orbital elements is computed. Finally, a normally distributed noise is added to the positions, which are then stored in the matrix **psdObs**. These positions serve as pseudo-observations for the following orbit determination. You will only process the first two hours of observations.

- (a) Perform a conventional least-squares solution of the orbit determination problem. Solve for the orbital elements and additionally for pulses in the velocity direction at every measurement epoch. Use the pseudo-observations in **psdObs** with equal weighting and introduce the orbital elements of the unperturbed orbit (defined at the beginning of **ex2.m**) as a priori elements. Perform the following steps:
  - Loop over all epochs. For each epoch:
    - Compute the satellite position of the a priori orbit using the function **ephem** and the a priori orbital elements (propagation in the two-body problem).
    - Compute the partial derivatives of the positions and velocities of the a priori orbit w.r.t. the orbital elements (using the function **rvpder**).
    - Compute the (constant) coefficients  $\beta_k$ ,  $k = 1, \dots, 6$ , which allow to express the partial derivatives of the orbit w.r.t. the pulses as a linear combination of the partials w.r.t. the six orbital elements.
    - Compute the ‘observed minus computed’ term and the first design matrix.
  - Set up the normal equation system.
  - Add the weights on the normal equation system to constrain the pulses towards zero.
  - Solve the normal equation system.

How many parameters do you solve for? How big is the normal equation matrix? What is the estimated value for the first pulse?

- (b) Plot the estimated pulses when using different a priori standard deviations **sig0** for the pseudo-observations (e.g., **sig0** = 1 and **sig0** =  $10^{-7}$ ). Read in the accelerations in the file **GRCA.ACC** and transform them into velocity changes. Plot these together with the estimated pulses. What changes if you change **sig0**?
- (c) Compute and plot the orbit residuals and the differences of the improved orbit w.r.t. the true orbit for all epochs in the geocentric (x,y,z) frame. Here you cannot compute the ‘true’ residuals by taking the updated orbital elements and propagating the new orbit (as you did in the second part of exercise 1d), since for the propagation you would need a numerical integration that takes the acceler-

ations in **GRCA.ACC** and the estimated pulses into account. Hence, compute the residuals of the linearized problem. Likewise, for the orbit difference add the (linearized) orbit corrections (computed by using the solution of exercise 2a to the a priori orbit (obtained by propagating the elements **eleTru** using the function **ephem**) and compare these positions with the true positions in the file **STOCH\_ORBIT**. Make again experiments with different values of **sig0**.

- (d) At each epoch the pseudo-stochastic pulse induces a change in the initial conditions (defined at the initial epoch). Compute and plot the difference of the epoch-specific semi-major axis w.r.t. the a priori value. Compare this difference with the difference of the true osculating semi-major axis w.r.t. the a priori value (in **difOsc**). Do this for different values of **sig0**.
- (e) Perform a filter solution of the orbit determination problem with only six unknowns by pre-eliminating the pulses every epoch. Initially, this is not possible, since for each new epoch all pulses up to this epoch will contribute to the observation equation. The pre-elimination becomes, however, possible when conducting a parameter transformation discussed in Sects. 2.3.3.3 and 2.3.3.4. Use the pseudo-observations in **psdObs** with equal weighting and introduce the orbital elements in **eleTru** as a priori values. In a loop over all epochs, perform the following steps:
  - Compute the satellite position using the function **ephem** and the a priori orbital elements.
  - Compute the first design matrix using the function **rvpder**.
  - Compute the ‘observed minus computed’ term.
  - Update the normal equation system with the observation equations of the current epoch.
  - Perform the parameter transformation, add the pseudo-observation for the pulse (with the corresponding weight) and pre-eliminate the pulse.
  - Generate and save the solution for the orbital elements, the residuals and the orbit difference w.r.t. the true orbit.

What are the estimated values of the orbital elements after the 5th filter step?

- (f) Compute and plot the real-time semi-major axis, the orbit residuals and the differences w.r.t. the true orbit in the geocentric  $(x,y,z)$  frame for each filter step.

Global Gravity Field Modeling from Satellite-to-Satellite  
Tracking Data

Naeimi, M.; Flury, J. (Eds.)

2017, XV, 168 p. 35 illus., 25 illus. in color., Hardcover

ISBN: 978-3-319-49940-6